frontiers in Physics

REVIEW
published: 28 March 2022
doi: 10.3389/fphy.2022.862962

Fundamentals and Applications of Topological Polarization Singularities

*Feifan Wang [1], Xuefan Yin[2], Zixuan Zhang[1], Zihao Chen[1], Haoran Wang[3], Peishen Li[1], Yuefeng Hu[3,4], Xinyi Zhou[1] and Chao Peng[1,3]**

[1]State Key Laboratory of Advanced Optical Communication Systems and Networks, School of Electronics and Frontiers Science Center for Nano-optoelectronics, Peking University, Beijing, China, [2]Department of Electronic Science and Engineering, Kyoto University, Kyoto, Japan, [3]Peng Cheng Laboratory, Shenzhen, China, [4]Peking University Shenzhen Graduate School, Shenzhen, China*

Radiations towards the continuum not only brings non-Hermicity to photonic systems but also provides observable channels for understanding their intrinsic physics underneath. In this article, we review the fundamental physics and applications of topological polarization singularities, which are defined upon the far-field radiation of photonic systems and characterized by topological charges as the winding numbers of polarization orientation around a given center. A brief summarizing of topological charge theory is presented. A series of applications related to topological polarization singularities are then discussed.

Keywords: topological charges, topological photonics, bound states in the continuum, optical singularities, non-Hermitian optics

OPEN ACCESS

Edited by:
Guancong Ma,
Hong Kong Baptist University, Hong Kong SAR, China

Reviewed by:
Cuicui Lu,
Beijing Institute of Technology, China
Yi Xu,
Guangdong University of Technology, China

****Correspondence:***
Chao Peng
pengchao@pku.edu.cn

Specialty section:
This article was submitted to Optics and Photonics, a section of the journal Frontiers in Physics

Received: *26 January 2022*
Accepted: *24 February 2022*
Published: *28 March 2022*

Citation:
Wang F, Yin X, Zhang Z, Chen Z, Wang H, Li P, Hu Y, Zhou X and Peng C (2022) Fundamentals and Applications of Topological Polarization Singularities. Front. Phys. 10:862962. doi: 10.3389/fphy.2022.862962

1 INTRODUCTION

Waves are ubiquitous phenomena in the nature. Serving as one of the most fundamental concepts in modern physics and applications, the examples range from electromagnetic waves, acoustic waves, to matter waves. Ever since the discovery of the transverse nature of some waves, the study of the polarization properties of those vector waves has attracted a great deal of attention, and varieties of novel mathematical concepts have been introduced. Among them, the most direct representation of polarization is the elliptically polarized state. For a generic plane wave, its field vector can be traced from the evolution of amplitudes and phases along two orthogonal directions, and correspondingly, the wave motion becomes a rotating vector that follows an ellipse path. In addition, the complicated polarization states can be projected onto the Poincaré sphere for better visualization, by using the Stokes' parameters [1]. Such a geometric representation shed lights upon deeper understanding of polarization from topological perspectives [2].

From a topological point of view, the objects of interest are some special points or regions on the Poincaré sphere, known as the singularities, such as lines where the polarization gets linear ("*L* lines"), points with circular polarization ("*C* points"), and centers of polarization vortices ("*V* points") [2–6]. At these regions, one or two components that compose the polarization, namely amplitude and phase, are ill-defined, so that the waves may exhibit some abnormal behavior, leading to exotic and potential useful physical phenomena. In particular, a special attention has been paid to the realization of singularities in optical domain [2, 6–9]. Examples include optical vortex beam generation [10–12], cylindrically polarized laser beams for tighter focusing [13–16], and the bound states in the continuum (BICs) [17–20]. It is noteworthy to highlight the BICs. Although the BICs have been developed from different contexts in history, their nature was found to be topological. Since first proposed in 1929 by von Neumann and Wigner [21], the BICs are understood as an

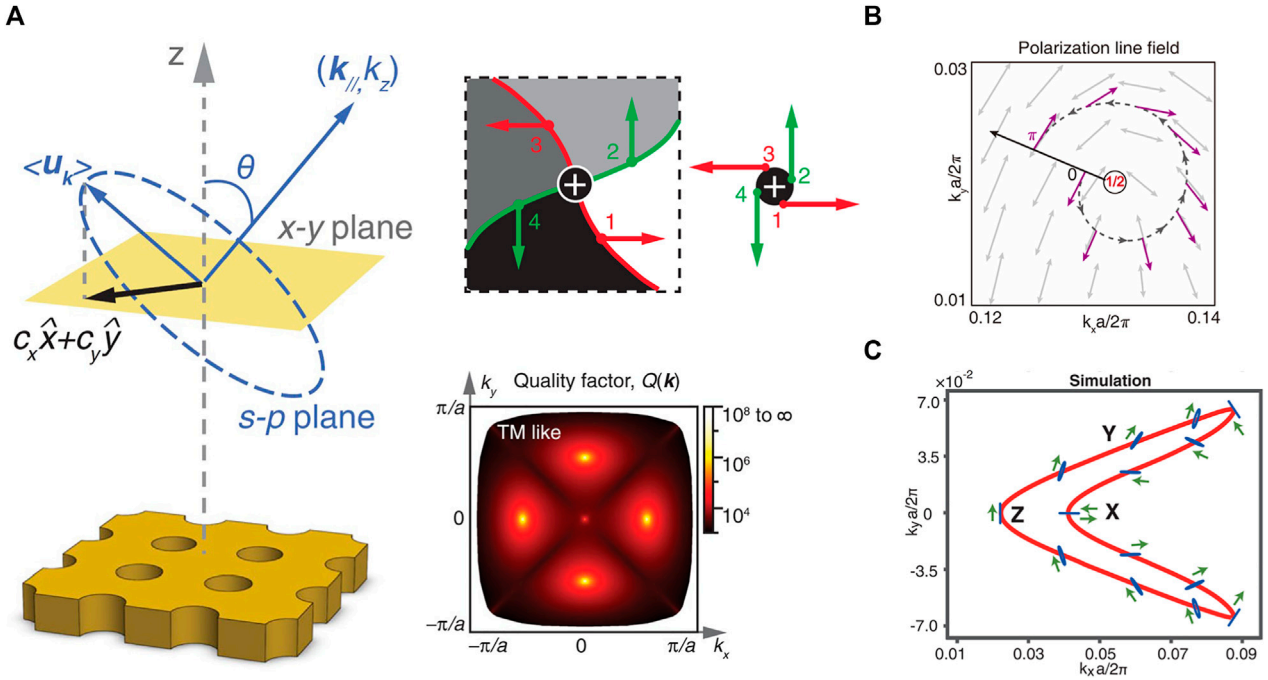

FIGURE 1 | Definitions and properties of different types of polarization singularities, **(A)** BICs [25] copyright American Physical Society; **(B)** a CP with charge +1/2 [43] copyright Springer Nature Ltd., and **(C)** a bulk Fermi arc connecting paried EPs [26] Copyright AAAS.

elimination of radiation in the case that radiation is allowed. After the first photonic realization [22], the BICs had been intensively investigated in various systems from a picture of destructive interference of waves [17, 18, 23, 24].

Later, the topological picture regarding BICs was established: they are interpreted as the vortex centers in far-field polarization orientation field where the polarization is ill-defined and all the radiation is forbidden [25]. In other words, BICs are a type of *V*-points in *k*-momentum space. By counting on the winding times of polarization direction around a specific center in momentum space, a conserved quantity called "topological charge" was defined, which was proved to be a topological invariant. It is found that the BICs possess integer topological charges [25]. Besides, the circularly-polarized states (CPs) carry half-integer topological charges, as a type of *C*-points. Furthermore, the topological charges defined on polarization are connected to the non-trivial band topology of non-Hermitian systems: half charges have been observed from a bulk Fermi arc encircling paired exceptional points (EPs) [26]. These findings built a framework to understand the polarization singularities, and utilize them for many applications.

In this article, we review the fundamental physics and applications of the research field of topological polarization singularities. We start from briefly summarizing the general principles and theory framework, and then present a comprehensive review on a series of applications related to polarization singularities. At last, we give our prospect and summary.

2 PRINCIPLES AND THEORY

The concept of optical singularities provide vivid and useful representations to understand the exotic phenomena of light, and thus they are applied in a series of investigation for different purposes. To keep the review focused, we concentrate on topological polarization singularities in this article. Specifically, we review the theoretical framework of polarization topological charges in this section, including their definitions, origins, and the methods for manipulating them. More information and connections regarding related topics can be found in other review articles, including topological photonics [27–29], singular optics [2, 6, 7], non-Hermitian topology [30–36], BICs [37–39], and orbital angular momentum of light (OAM) [40–42].

2.1 Theory of Polarization Topological Charges

Polarization topological charge was firstly proposed to depict the topological nature of BICs. In 2014, Zhen et al. [25] pointed out that the BICs are *V*-points in the far-field polarization vector field, carrying integer topological charges in momentum space. At the vortex center, the radiation is eliminated since the far-field polarization cannot be defined. **Figure 1A** illustrates the basic concepts of BICs. A resonance turns into a BIC if and only if $c_x = c_y = 0$, where (c_x, c_y) is the projection on the x-y plane of electric field $< u_k >$ of the radiative wave. The polarization field winds according to the topological charge, and *Q* diverges at BICs. An

explicit definition of the polarization topological charge is given by:

$$q = \frac{1}{2\pi}\oint_C d\mathbf{k} \cdot \nabla_{\mathbf{k}}\phi(\mathbf{k}) \quad (1)$$

in which $\phi(k)$ is the angle of the polarization vector arg $[c_x(\mathbf{k}) + ic_y(\mathbf{k})]$ describing the orientation of polarization major axis, $\mathbf{k}$ is the in-plane wavevector, and C is a closed simple path in momentum space that goes around a specific point along the counterclockwise direction. **Eq. 1** describes the number of times that the polarization vector winds around the specific point in momentum space. Encircling the BICs, namely the vortex centers, the polarization vector has to come back to itself after travelling through a closed loop, upon which the topological charge q must be an integer. Besides, according to the definition, we readily check that the CPs carry half-integer charges as $q = \pm 1/2$ from a topological view. **Figure 1B** gives a possible configuration of the polarization field near a CP, giving rise to a topological charge $q = +1/2$. Both the BICs and CPs are types of topological polarization singularities.

Note that the polarization topological charge is defined upon the far-field polarization in momentum space, which may connect, or say project the intrinsic band topology to the radiation field. For example, half-integer charges was observed around the bulk Fermi arc (**Figure 1C**), as a direct consequence of paired EPs [26] revealing the non-Hermitian topology of the bulk bands. However, the connection between band topology and radiation topology may not be obvious. For instance, the BICs and CPs are polarization singularities in radiation field, but they are topologically trivial upon the energy band. Further explorations are for sure interesting topics.

As a topological invariant, topological charges are conserved quantities: they continuously evolve in the momentum space and cannot suddenly disappear unless one charge drops out of the light cone or annihilates with another charge with the opposite sign. Besides, a pair of half charges can merge to an integer charge, or annihilate to nothing according to their signs. Consequently, the topological charge evolution offers an abstract but essential view to understand the radiation characteristics, as well as new methods to manipulate it. Examples and consequences of charge evolution will be presented in the following section.

Topological charge is actually a quite general concept that can quantitatively depict the winding of any arbitrary attributes. Although sharing the same terminology, the term "topological charge" are not only defined on the polarization, but also on phase, or other attributes of wave, in the real space, momentum space or parameter space. It is worthy to pay extra attention to distinguish the definitions. For instance, the term has been applied to phase singularities [44–51] that are related to vortex beam generations, and singularities on transmissions or reflections [52–55]. Other definitions utilizing the concept of winding are also reported in electromagnetic [19, 56–58], phononic [59] and mechanical systems [60].

2.2 Origins of Integer Topological Charge

The BICs, which are polarization singularities carrying integer charges, have been an attractive topic for several decades. The history, origins and results of BICs have been comprehensively reviewed by Hsu et al. [37] in 2016. In this section, we will summarize the new advances and understandings developed in recent years. Given that the investigations upon the BICs are diverse and extensive, we organize our review from different aspects.

From the aspect of physics origins, Friedrich and Wintgen presented a fundamental picture of interfering resonances to create the BICs [61]. Their original work pointed out that, the coupling between any two or more leaky resonances could eliminate the radiation of particular hybridized resonances, if the coupling strengths were well chosen. Although the term "FW BIC" is currently usually specialized to a BIC raised from interband coupling, other types of BICs can also be interpreted from Friedrich and Wintger's picture, if one appropriately defines the "resonances". For instance, for a photonic crystal (PhC) slab or gratings system, such resonances are guided-mode resonances [62–67]; for nanoparticles, dielectric spheres or tight-binding metasurfaces, the resonances are Mie resonances or other localized states [68–70]; for metallic systems, they are plasmonics resonances [20, 71]. Accordingly, BICs can be explained as the hybridization of different bases (i.e. unperturbed resonances) equivalently from a mathematical point of view. Examples include the coupled-wave theory that uses quasi-plane waves as the bases in periodic structures [17, 23, 24], and the multipole-expansion theory for Mie resonances in which the shape of a single resonator matters [72–74].

From the aspect of system symmetry, the BICs are classified into "symmetry-protected BICs", and "symmetry-incompatible BICs" [17, 37]. Since the radiation elimination originates from the high symmetry, the symmetry-protected BICs usually reside at the symmetry center in momentum space (for instance the Γ point). It is noteworthy that the symmetry-protected BICs have been independently developed in different photonic fields in history and described by different terminologies, such as band-edge modes in distributed-feedback lasers (DFB) [75–79], and photonic-crystal surface emitting lasers (PCSELs) [78, 80–83]. On the other hand, the symmetry-incompatible BICs also have many alias names, such as tunable BICs [24], off-Γ BICs [23], resonance trapping BICs [84], and topology-protected BICs [25, 85]. Since the creation of symmetry-incompatible BICs doesn't rely on the in-plane symmetry, they can move off the symmetry center in momentum space, which is distinguishable from the symmetry-protected ones.

From the aspect of platforms, the BICs are realized in both periodic and non-periodic structures. PhC is an easy-to-fabricate, optical-friendly platform to investigate BICs and other polarization singularities, in which the lattice periodicity offers naturally well-defined Bloch bases to depict the wave interactions [20, 86, 87]. Compared with PhCs, metasurfaces [68–70], coupled arrays of rods [19, 88, 89] and spheres [85, 90] share some similarities in their geometries: both of them are periodic and planar. The major difference might be—while the PhC supports long-range interactions, the wave interactions in metasurfaces are likely short-ranged and dominated by a few of adjacent unit cells. Alternatively, another type of systems is single resonators [18, 91, 92]. Although in principle a perfect BIC cannot be realized in a

three-dimensional compact volume [37, 93], the single resonators can support quasi-BICs with considerably high-Q and extremely small modal volume V, thus they are promising for nonlinear optic application and sensing.

It is noteworthy that, the BICs with high-order topological charges $|q| > 1$ are also reported. The vortices with $q = -2$ were found in a triangular latticed PhC slab [20] owing to the high in-plane symmetry of the lattice at the high-order Γ point although not been explicitly mentioned. In 2020, Yoda et al. [94] reported a symmetry-protected BIC with charge $q = -2$ in a C_6 symmetric lattice. It was found that two BICs each with $q = -1$ spawned from the $q = -2$ charge when the in-plane symmetries were broken from C_6 to C_2.

Another interesting fact is, although the BICs are usually isolated points, they can appear as a line in momentum space when involving extra dimensions. In 2019, Cerjan et al. [95] proposed a method called the environmental design for this purpose, in which the environment worked as new degree of freedom. Recently, this line of BICs was observed in a slab by altering the surrounding radiative environment with a 3D PhC [96].

Moreover, the topological polarization singularities are found in other systems such as disordered or quasi-crystal systems, and parity-time-symmetric (PT-symmetric) systems. In 2019, De Angelis et al. [97] reported the random vortices in a chaotic cavity composed of 2D PhCs. In 2021, Che et al. [98] experimentally observed the quasi-BICs in 2D photonic quasi-crystals. In 2020, Song et al. [99] reported the emergence of two types of modes with divergence of Q in a PT-symmetric system, named as a "PT-BIC" and a "lasing threshold mode".

2.3 Emergence of Half-Integer Topological Charge

Another type of polarization singularities, namely CPs, can also emerge in momentum space by tuning material or structural parameters. According to the definition of topological charges, the CPs carry half-integer charges that obey the conservation law of topological charge together with the integer charges. Several methods are reported to create these half charges.

One method is to split integer charges to paired half charges following the conservation law, for instance $q = 1 \rightarrow 1/2 + 1/2$, by breaking the in-plane symmetry. As reported by Liu et al. [100], it was observed that a symmetry-protected BIC split into a pair of CPs with opposite helicity but carrying topological charges of the same sign. Similar phenomenon was observed by Chen et al. [71]. The CPs can also originate from symmetry-incompatible BICs. For instance, Ye et al. [101] reported two CPs with identical topological charges of $q = -1/2$ but different handedness originating from a BIC with charge $q = -1$ at the K point in a honeycomb-lattice PhC. As mentioned above, Yoda et al. [94] showed that the BIC with high order charge $q = -2$ split to integer charges following $q = -2 \rightarrow (-1) + (-1)$ by breaking the symmetry from C_6 to C_2. By further breaking the C_2 symmetry, the integer charge split to paired half charges as $q = -1 \rightarrow (-1/2) + (-1/2)$. It is noteworthy that all the evolution followed the conservation law.

An alternative method for creating half charges is to spawn the CPs from trivial polarization field, namely $q = 0$. Recently, Zeng et al. [102] built a two-layered 1D PhC with an offset between the layers. Two CPs emerged from a given k point where the far-field polarization is trivial, carrying opposite signed half charges as $q = 0 \rightarrow 1/2 + (-1/2)$. Apparently, the conservation law still held.

Besides, polarization half charges are related to another important type of singularities in non-Hermitian system, namely EPs. In 2018, Zhou et al. [26] reported a pair of EPs connected by so-called bulk Fermi arc. A flip of the polarization major axis was observed in experiment along one closed loop around the EP pair connected by bulk Fermi arc, showing a clear signature of polarization half charge. It is noteworthy that the EPs belonged to the singularities upon the non-Hermitian band, while the polarization half charges represented the singularities upon the radiation. It is still vague that how the band topology connects to the radiation topology. Nevertheless, as reported by Chen et al. [103], a conservation law of global charge was still valid.

2.4 Consequences of Topological Charge Evolution

The conservation law of topological charges allows the continuous evolution of charges in momentum space, namely moving, merging, splitting and annihilating with the summation of all charge numbers remaining constant. Since the topological charges are related to the far-field radiation characteristics, it was found that interesting and useful consequences could be obtained from the topological charge evolution.

One of the example is the merging of multiple integer topological charges, i.e. the BICs, which strongly suppresses the out-of-plane scattering and leads to a class of robust ultra-high-Q resonances. Although the BICs completely forbid the radiation and own infinite photon lifetime in theory, their experimental realizations had suffered from a limited Q in a level of 10^4 [17], due to the energy leakage from the inevitable out-of-plane scattering originated from fabrication imperfections. To address this problem, Jin et al. [104] reported a method of merging BICs in a C_4 symmetric PhC slab where existed eight off-Γ BICs with $q = \pm 1$ charges around one symmetry-protected BIC at the Γ point. By continuously tuning the lattice periodicity a, the eight BICs kept moving until merging at Γ, and further annihilated into one isolated BIC with charge $q = +1$. (**Figure 2A**).

As mentioned, the configuration of topological charges implies the radiation capabilities of nearby resonances, and further determines the observable Qs in samples by taking into account the scattering losses. Near an isolated BIC with charge $q = \pm 1$, the Q scales quadratically ($1/k^2$) as the distance k away from the BIC. However, the scaling law dramatically changes to $1/k^6$ when nine BICs just merge, as shown in Jin's work. As a result, the scattering loss was significantly suppressed, and a record-high Q of 4.9×10^5 was experimentally observed.

Recently, Kang et al. [105] took a further step and realized a merging BIC at off-high symmetry points, namely the merging

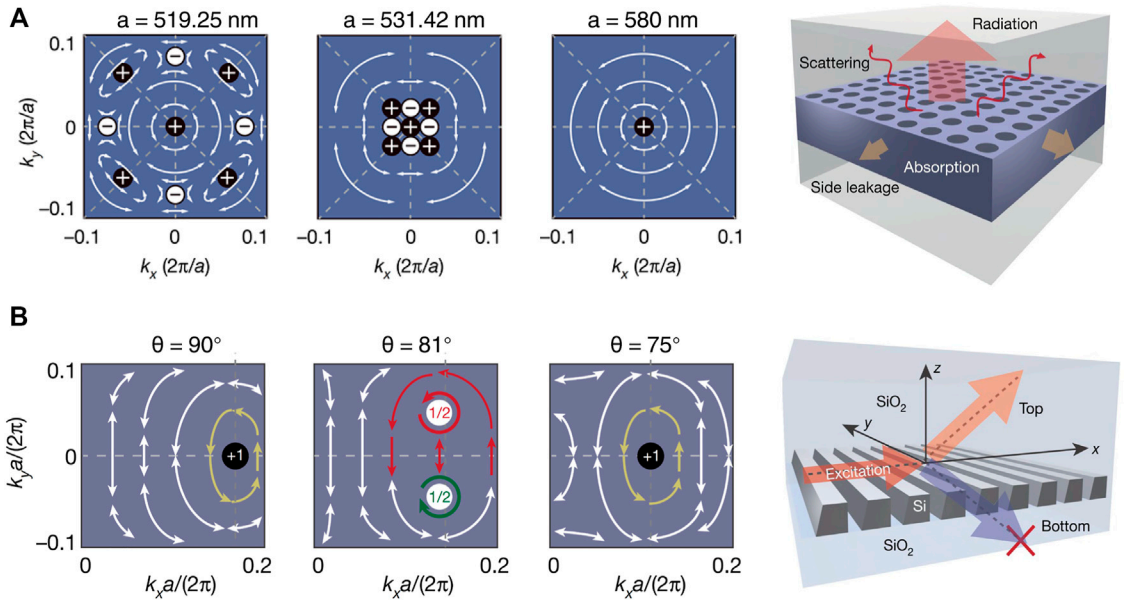

FIGURE 2 | Consequences of topological charge evolution. **(A)** A high-*Q* cavity robust of out-of-plane scatterings constructed by the merging of multiple integer charges [104]. **(B)** The merged half-charges in downward radiation leading to a unidirectional radiation [43]. Copyright Springer Nature Ltd.

behavior of integer charges were not restricted to the Brillouin zone (BZ) center. The in-plane C_4 and mirror symmetries were broken, resulting in the merging of an FW-BIC and a tunable-BIC at a nearly arbitrary point in momentum space.

Another example of topological charge evolution is related to an interplay with half charges and integer charges, leading to the realization of unidirectional guided resonances (UGRs) (**Figure 2B**), reported by Yin et al. [43]. The evolution started from an off-Γ BIC in a 1D silicon PhC slab, carrying a topological charge of $q = +1$ upon both up- and downwards radiation. By tilting the sidewall that broke the in-plane C_2 symmetry and up-down mirror symmetry simultaneously, the BIC split into a pair of CPs carrying $q = +1/2$ upon both the top and bottom sides of the slab. Further, paired CPs evolved following different trajectories in the upward and downward radiation fields due to the breaking of up-down mirror symmetry. At a specific angle, the paired CPs in downward radiation merged into an integer charge while upward CPs remained departing. Therefore, the downward radiation was totally eliminated while the upward radiation channel was still open, thus generating a resonance with directional emission named UGR. The experimental results demonstrated 99.8% of the energy radiated through the upward channel at UGR.

Recently, Zeng et al. [102] reported a similar phenomenon from theory in a two-layered 1D PhC with an offset between the two layers which broke the up-down-mirror symmetry. Two pairs of CPs with $q = \pm 1/2$: one left-handed pair and another right-handed pair, emerged at a specific value of the offset. By continuously varying the offset, the CPs evolved in momentum space, and merged to integer charges at different k points upon up- and downward radiation, which created two UGRs.

3 APPLICATIONS

Topological charge provides not only a convenient mathematical tool in theory, but also flexible and rich methods for manipulating lights, thus paving the way to a variety of applications. In particular, topological charges can be tuned to selectively eliminate or suppress the radiation, which leads to the realization of optical modes with ultra-long lifetime and desired radiation patterns in intensity, phase and polarization. Consequently, topological charges have been applied in many scenarios, boosting the development of light trapping, lasing, light-matter interaction enhancement, nonlinear optics, wavefront control, polarization conversion, photonic integration and others. In this section, we review the recent progresses of applications related to the topological charges.

3.1 Trapping of Light and Optical High-*Q* Cavities

From a scientific or technological point of view, the importance of light-trapping is self-evident. The BICs are interpreted as vortices in far-field polarization, thus providing novel methods for light-trapping other than conventional optical cavities such as bound states under light-cone [108–110].

Early efforts was paid to inhibit out-of-plane radiations in large-area 2D systems. In 2012, Lee et al. [106] reported observation of a unique high-*Q* resonance near zero wavevector in large-area 2D PhC slab by using angular resolved analysis. *Q* of 1×10^4 was found near the symmetry-protected BIC at Γ point (**Figure 3A**). In 2013, Hsu et al. [17] reported the off-Γ BICs for the first time, in which the *Q*s of resonances diverge to infinity at seemly insignificant wavevectors

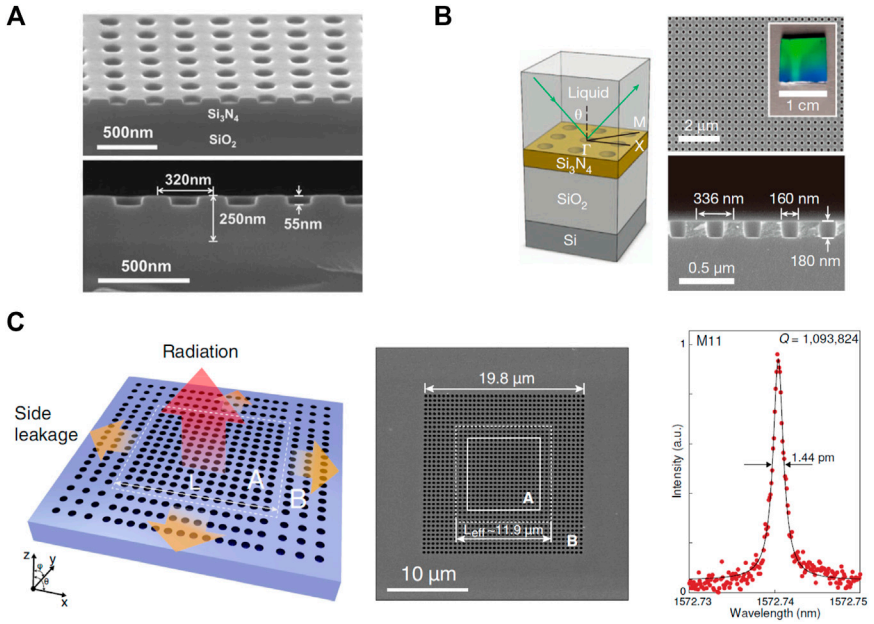

FIGURE 3 | (A) Macroscopic photonic crystal [106] for observing symmetry-protected BICs, copyright American Physical Society. **(B)** The observation of symmetry-incompatible off-Γ BICs [17], copyright Springer Nature Ltd. **(C)** Miniaturized BICs [107], copyright Science China Press.

on certain bands. The structure is shown in **Figure 3B**. A radiative quality factor Q_r of 1×10^6 was measured at a direction angle ~ 35° of the reflection. Such BICs can stably exist in a general class of geometries and can move to a different k point by continuously tuning the system parameters.

Subsequently, Zhen et al. [25] proposed the topological interpretation of the BICs in 2014 as elaborated in previous sections. The BICs' capability of trapping light are further promoted. In 2019, Jin et al. [104] proposed and realized a class of ultra-high-Q resonances by merging multiple off-Γ BICs carrying topological charges towards the center of Brillouin zone (BZ). As a direct consequence of topological charge manipulation, Qs as high as 4.9×10^5 were observed in an SOI PhC slab, as mentioned in **Section 2.4**. The merging-BIC designs strongly suppressed out-of-plane-scattering losses caused by fabrication imperfections, thus paved the way to realistic applications of BICs.

Strictly speaking, all the above examples belong to high-Q resonances but not high-Q cavities. According to the continuity of electromagnetic field, it was proved that fully 3D compact BIC does not exist in theory [37, 93]. In addition, the periodic conditions of PhC imply that the structure extends infinitely in the lateral direction, which is not practically feasible. The high-Q resonances in PhC slabs only localize in the vertical direction but remain de-localized in transverse direction across the slab.

The most straightforward method for achieving 3D light-trapping is to simply truncate the PhC slab laterally. Such method reduces modal volume V but also drastically degrades the quality factor Q because it introduces leakage in both lateral and vertical directions. A common relationship between Q and V for truncated BICs was derived [111] and verified experimentally [112]. In 2019, Liu et al. [69] observed a truncated BIC with Q of 18,511 and footprint of $19 \times 19\,\mu m^2$. In 2021, a long-lifetime mode with Q of 7,300 was reported in InGaAsP PhC slab for low-threshold lasing in a footprint of $22.4 \times 22.4\,\mu m^2$ [113]. In addition to simply truncating the PhC, the light can be confined transversely by applying lateral hetero-structures as reflective perimeters. For example, a mode with Q of 2×10^4 has been measured in footprint of $215\,\mu m^2$ [114]. In these designs, although the hetero-structure suppress the lateral energy leakage effectively, the leakage toward out-of-plane direction raised by truncation remains unresolved.

Recently, Chen et al. [107] reported a new method of light trapping combining lateral mirrors and BIC in a cooperative way (**Figure 3C**). Light was confined in the vertical direction by manipulating the constellation of topology charges, matching them with the finite-size radiation channel. In the transverse direction, the light was trapped by the near-perfectly reflective photonic bandgap of the lateral hetero-structure, with the radiative and scattering losses of the boundary region being greatly suppressed, at the same time, the radiation in cavity region becomes highly directional. The coworking of the topological-charges covered a larger area in momentum space that protects the scattered waves from radiation. Since the boundary region shared similar geometries with the cavity region, they also benefit from the protection of topological constellation for a smaller radiation loss. As a result, light-trapping in all three dimensions was achieved. Miniaturized BICs with Qs of 1.09×10^6 was measured experimentally with a footprint of ~ $20\,\mu m \times 20\,\mu m$. Benefiting from the protection of topological constellations that are composed by topological

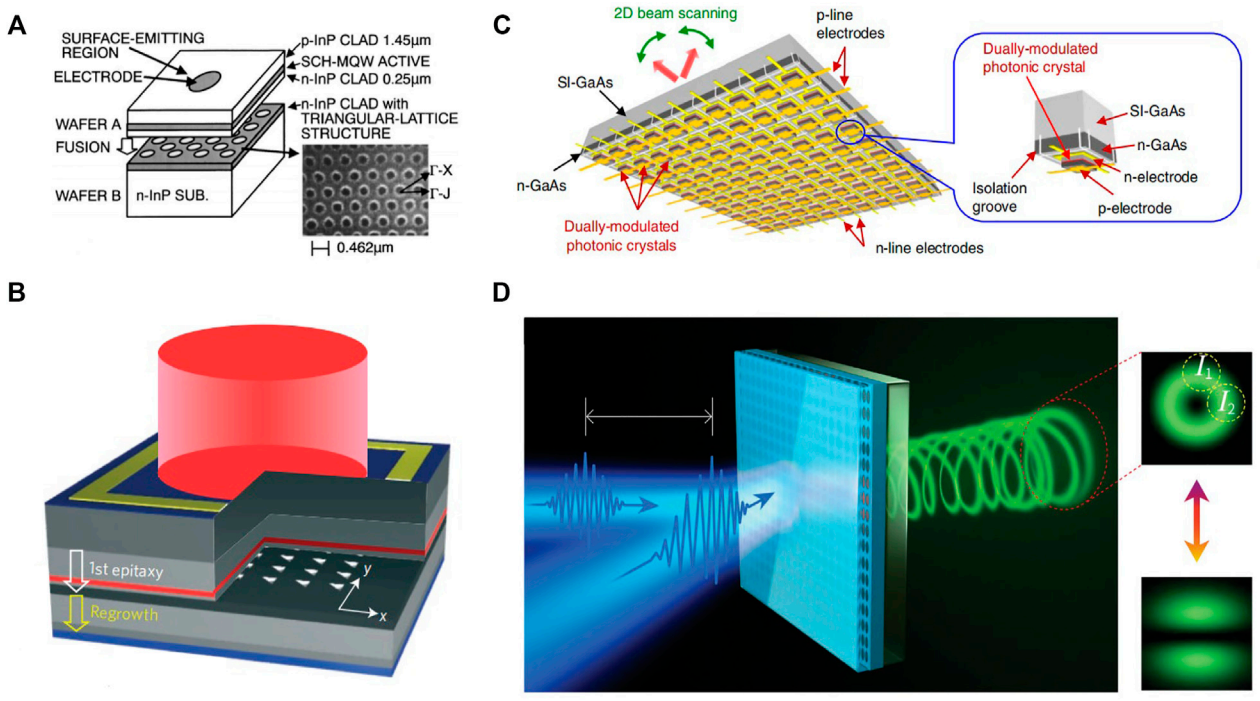

FIGURE 4 | (A) Early PCSEL based on wafer fusion technique [80], copyright AIP publishing. **(B)** A W-class high-power PCSEL [82], copyright Springer Nature Ltd. **(C)** The on-chip beam scanning laser [123], copyright Springer Nature Ltd. **(D)** All-optical switching from the vortex microlaser [124], copyright AAAS.

charges, the microcavity exhibited excellent robustness to fabrication imperfections.

3.2 Lasing and Vortex Beam Generation

Since the integer topological charges carried by BICs are good candidates for realizing high-Q resonances, their most direct application is for lasing. Historically, the band-edge modes were widely adopted for semiconductor lasers such as DFB lasers [75–79] and distributed Bragg reflector (DBR) lasers [115–117]. Although it is not explicitly mentioned, the grating modes that operate at the band-edge of second-order Γ point are actually the symmetry-protected BICs. Later, the periodicity of one-dimensional gratings was extended to two-dimensional PhC slabs, leading to the invention of photonic-crystal surface-emitting lasers (PCSELs) [80]. The PCSELs also operate near the band edge residing in the continuum, supporting coherent oscillations in large areas. In the case that the periodic lattice and unit cells of PCSELs respect C_2 or higher in-plane symmetry, the lasing band-edge modes are found to be symmetry-protected BICs, too [118, 119].

In the past two decades, PCSELs have experienced dramatically developments and become a promising laser architecture as the successor of DFB lasers which had already made tremendous successes in industry. With a comprehensive review of PCSELs presented elsewhere [120], here we just list several major milestones: the first lasing action of PCSELs was observed in 1999 [80], as illustrated in **Figure 4A**; room-temperature, continuous-wave operation, current-injected lasing was achieved in 2004 [81]. Later, the abilities of tailoring beam patterns were reported in 2006 [121]; the lasing wavelength was extended to blue-violet region in 2008 [78]; a beam-steering functionality was demonstrated in 2010 [118]. What's more, much efforts have been paid to promote the lasing power, and watt-class lasing was achieved (shown in **Figure 4B**) in 2014 [82] and 10-W-class lasing in 2019 [83]. Recently, PCSELs with a peak power of 20 *W* and pulse width of 35 *ps* were realized [122] and on-chip beam scanning lasers were first achieved [123] as illustrated in **Figure 4C**. It is noteworthy that, in the early age of PCSELs, circular shaped holes were adopted to pattern the PhC, so that the lasing modes were the BICs with infinite Qs in theory. Although the high Q factor lowered the lasing threshold, it was not good for high-efficient power extraction which was critical for high-power lasers. Therefore, the in-plane C_2 symmetries were broken on purpose, which turned the BICs with infinite Qs to quasi-BICs with high but finite Q values in carefully controlled manners [82, 83].

Besides the PCSELs, the lasing action utilizing the BICs have also been developed in a parallel lane motivated from physics curiosity. In 2017, Kodigala et al. [84] demonstrated the optical-pumped lasing in an array of suspended cylindrical nanoresonators consisting of $In_xGa_{1-x}As_yP_{1-y}$ multiple quantum wells, claimed as the first lasing action of the BICs. In 2018, Ha et al. [125] reported directional lasing in resonant semiconductor nanoantenna arrays, that is, arrays of GaAs nanopillars. On the other hand, lasing action has been reported in Mie-resonant BICs, too. For instance, combining colloidal CdSe/CdZnS core-shell nanoplatelets with square-

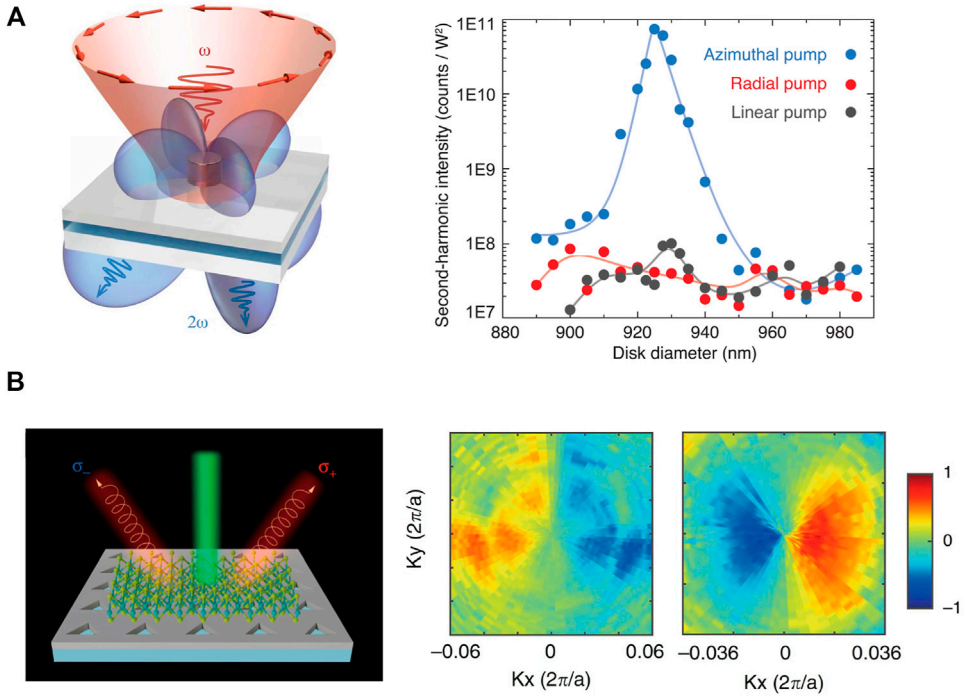

FIGURE 5 | Light-matter interaction enhancement and nonlinear optics. **(A)** SHG in an isolated antenna, the SH intensity vs nano-resonator diameter was measured at different pump polarizations [18], copyright AAAS. **(B)** Routing of valley photons with different chiralities by coupling to CPs, measured valley polarization in momentum space at 615 *nm* (left) and 628 *nm* (right) [129], copyright Springer Nature Ltd.

latticed TiO_2 nanocylinders, Wu et al. [126] reported the lasing from in-phased out-of-plane magnetic dipoles in 2020.

It is worthy to mention that, the polarization singularities accompanied with the BICs can be adopted to generate rich and exotic beam patterns. Some early experiments of PCSELs showed such possibility of creating tailored vectorial beams [121]. Recently, vortex beam generation has attracted huge attention, particularly owing to its great potentials in escalating the optical communication systems to higher level of multiplexing. In 2020, Wang et al. [12] reported optical vortex generation in a PhC slab with i-fold ($i > 2$) rotational symmetry related to the BICs, in which spin-to-orbit angular momentum conversion was realized and the vortex beam was proved to be a diffraction resistant high-order quasi-Bessel beam. Also in 2020, Huang et al. [124] reported that the BICs enabled ultra-fast control of vortex micro-lasers based on a perovskite metasurface, as shown in **Figure 4D**. Through modifying the two-beam-pumping configuration, ultra-fast switching between a vortex beam and regular linearly polarized beam was demonstrated with a transition time of only 1.5 ps.

3.3 Light-Matter Interaction Enhancement and Nonlinear Optics

As elaborated in **Section 3.1**, ultra-high Qs and small modal volume Vs can be achieved by arranging the topological charges, leading to dramatic enhancement of Purcell effect that favors the light-matter interactions and nonlinear optics. In 2019, Xu et al. [127] experimentally demonstrated third-harmonic generation (THG) in silicon metasurfaces and observed a conversion efficiency of 5×10^6 at $100\,mW$. Later, Liu et al. [69] promoted the Q to a record-high value of 18,511 in the metasurface, and reported that the THG conversion efficiency was five orders of magnitude higher than the former silicon metasurfaces. Even the second-harmonic generation (SHG) was also observed in silicon in their work. Moreover, Kang et al. [128] observed the high-order vortices, namely, high-order topological charges upon the harmonic waves generated from optical nonlinearity.

To enhance the efficiency of the nonlinear processes, several considerations were taken into account. Firstly, the excitation and emission of the resonances under critical-coupling condition would maximize the field strength in the cavity. As reported, by slightly breaking the in-plane symmetry that shifted the resonance away from the complete dark BIC, the energy exchange between the external excitation and the resonance became more efficient, thus promoting the conversion efficiency [127, 130]. Besides, the process benefited a lot from a doubly-resonant design, namely both the excitation and its harmonics were resonances supported by the same cavity. For example, Wang et al. [114] realized a GaN photonic cavity from this concept, in which the fundamental frequency matched with a

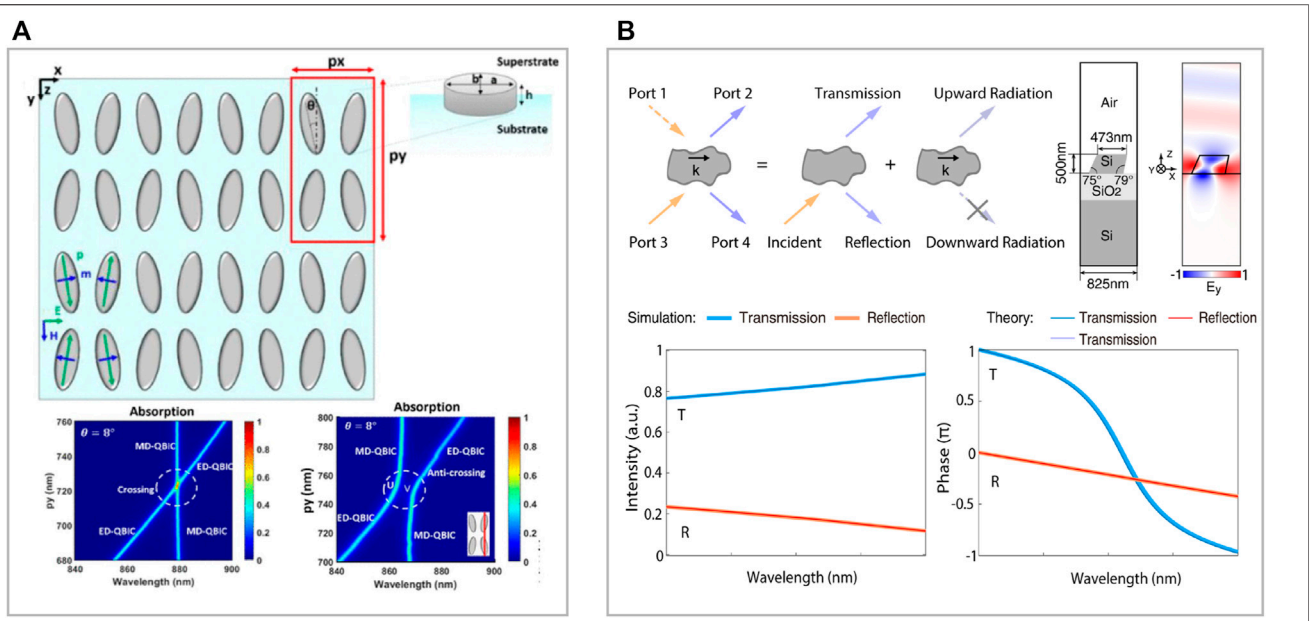

FIGURE 6 | Light manipulation in intensity and phase. **(A)** High-*Q* silicon metasurface and its absorption spectra [134], copyright American Chemical Society. **(B)** Intensity flatten phase shifting based on the unidirectional radiation resonance [135], copyright De Gruyter.

defect mode and its second-harmonics operated upon a quasi-BIC. As a result, the intrinsic conversion efficiency was 10 times larger than singly resonant cavities with similar materials.

Besides the periodic structures including PhCs and metasurfaces, single Mie resonators provide another promising platform for nonlinear optics. Although the *Q*s of single resonators are lower than that of periodic structures, single resonators have particular advantages in small modal volume *V* to promote the strength of light-matter interaction. In 2018, Carletti et al. [91] predicted that the conversion efficiency of SHG in an isolated AlGaAs nano-antenna could be two orders of magnitude stronger than that in conventional designs. In 2020, Koshelev et al. [18] experimentally implemented such design, as illustrated in **Figure 5A**. They found a quasi-BIC in a particle with a diameter of 930 *nm* and height of 635 *nm*. Owing to the mutual interference of several Mie modes, *Q* of 188 was realized. Combining with doubly-resonant strategy, two orders of magnitude higher conversion efficiency was achieved as expected.

In addition to those dielectric nonlinear materials, thin-film materials such as 2D transitional metal dichalcogenides (TMDCs) were specifically cooperated with the BICs to investigate the light-matter interaction. In 2018, Koshelev et al. [131] achieved a strongly-coupled exciton-photon system in which PhC was covered by a WSe_2 monolayer. Two years later, Kravtsov et al. [132] demonstrated a BIC-based polaritonic excitation with $MoSe_2$ upon PhCs, in which strong exciton-fraction-dependent optical nonlinearities were exhibited. Besides, as reported by Yu et al. [133], the decoupling from the continuum could confine light in a low-dielectric waveguide upon high-dielectric substrate, which contributed to new graphene device designs.

Besides the *V*-points (BICs), the *C* points (CPs) can also be involved in the light-matter interactions since they provide extra selectivity in chirality. In 2020, Wang et al. [129] generated paired CPs with different chirality. Owing to the valley-dependent selection rules in WSe_2, the photons radiated from inequivalent valleys could couple to the two CPs, as illustrated in **Figure 5B**. Accordingly, a maximum degree of valley polarization over 80% was observed.

3.4 Intensity and Phase Modulation

Amplitudes and phases are fundamental attributes depicting the characteristics of light. By cooperating with the resonances associated with topological charges, these attributes can be manipulated thus leading to a series of applications.

As a directly-observable attribute, the intensity of light can be controlled for a variety of purposes. Specifically, in 2019, Yu et al. [133] realized a BIC-waveguide-integrated modulator in which the electro-absorption effect of graphene was adopted and a bandwidth of 5 *GHz* was achieved. In 2020, Tian et al. [134] theoretically proposed that a near-unity absorption could happen on an all-dielectric metasurface with quasi-BICs, when the material absorption rate matched with the radiative decay rate (**Figure 6A**). Dai et al. [53] proposed a mechanism for perfect reflection called coherent perfect reflection (CPR), which was raised from interband coupling between two propagating modes so the forward transmission of light could be eliminated under appropriate complex coupling coefficients. Besides, Wong et al. [55] conceived an idea for perfect isolation of light from topological theory, upon a nonreciprocal metasurface composed of dimer unit cells interacting with a static magnetic field.

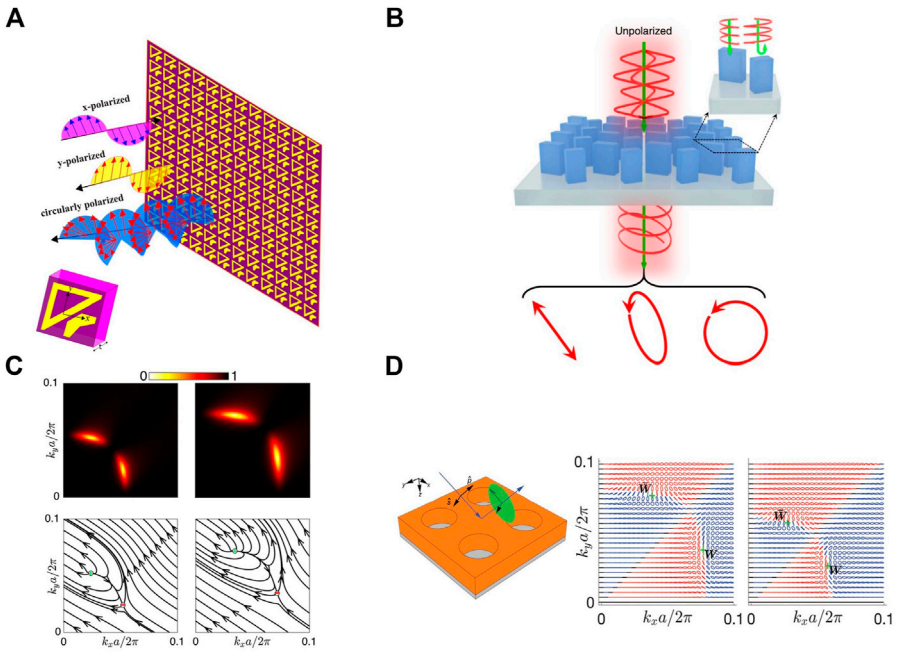

FIGURE 7 | (A) fish-like metasurface converting linear polarization to orthogonal-linear and circular polarization [142], copyright Springer Nature Ltd. **(B)** Dimerized nanopillars generating linear, elliptical and circular polarization regardless of input polarization [145], copyright Springer Nature Ltd. **(C)** Maps of reflection coefficient and vector field of reflection in momentum space in the polarization conversion [52], copyright American Physical Society. **(D)** PhC slab manipulating incident polarization to arbitrary polarization in reflection [146], copyright Wiley-VCH GmbH, Weinheim.

Besides, phase is also a key attribute of light that plays important roles in many scenarios. The modulation of phase is as straightforward as intensity, since both of them are related to the tuning of the resonances themselves. As an example, a thermo-optic phase-shifter utilizing the high-Q quasi-BICs was reported [136]. However, phase-only modulation, namely the phase modulation without the change of intensity, is even more important for applications ranging from three-dimensional video projection, flat metalens optics, to optical phased arrays and light detection and ranging.

Although perfect phase-only modulation is difficult, much effort was devoted for intensity-flatten phase modulation, with the key concept of making the resonance operating under over-coupled status. For instance, Kwon et al. [137] experimentally demonstrated nano-electromechanical tuning of gratings associated with quasi-BICs in the telecom wavelength. They realized a spectral shift over 5 nm, with absolute intensity modulation over 40%, modulation speed exceeding 10 kHz, and a phase shift of 144° with a bias of 4 V. Salary et al. [138] proposed an electro-optically tunable all-dielectric metasurface composed of elliptical silicon nanodisks for the same purpose. By applying bias voltage, the electro-optical driven Huygens mode produced a dynamic phase span of 240° while maintaining an average transmission amplitude of 0.77, giving rise to a unevenness of about 25%.

Recently, it was reported by Zhang et al. [135] that perfect phase-only modulation was possible in theory with the assistance of the UGRs (**Figure 6B**). As mentioned, UGRs are connected to single-sided topological polarization singularities. A UGR mandates the light transmitting to only one out-going port without other choices, which creates perfect phase-shifting upon the transmission if nonradiative loss is negligible. The unevenness of transmission intensity could be lower than 10% with nonradiative Q > 8,000 which was feasible in state-of-art fabrication process.

3.5 Polarization Conversion

Polarization is a critical and fundamental attribute of electromagnetic waves and the polarization control has been widely used in optical communications [139], nonlinear optics [140], imaging [141], etc. Besides cascading polarizers and waveplates to regulate the polarization, periodic structures including the metasurfaces and PhC slabs are promising platforms to achieve the polarization conversion [52, 139, 142–146], by manipulating the polarization singularities in radiation.

To be specific, Khan et al. [142] reported a single-layer, mirror-symmetric anisotropic metasurface constructed of fish-like unit cells to demonstrate both the linear cross-polarization conversion and linear-to-circular polarization conversion in X-band, as illustrated by **Figure 7A**. Besides, broadband linear-to-circular polarization conversion in the terahertz region with almost unity conversion efficiency was demonstrated by Chang et al. [144] based on the birefringent metasurface. In 2021, Wang et al. [145] proposed a monolayer all-dielectric metasurface composed of dimerized nanopillars shown in **Figure 7B**, which generated arbitrary polarization on the Poincaré sphere from the unpolarized input light. This effect was equivalent to an

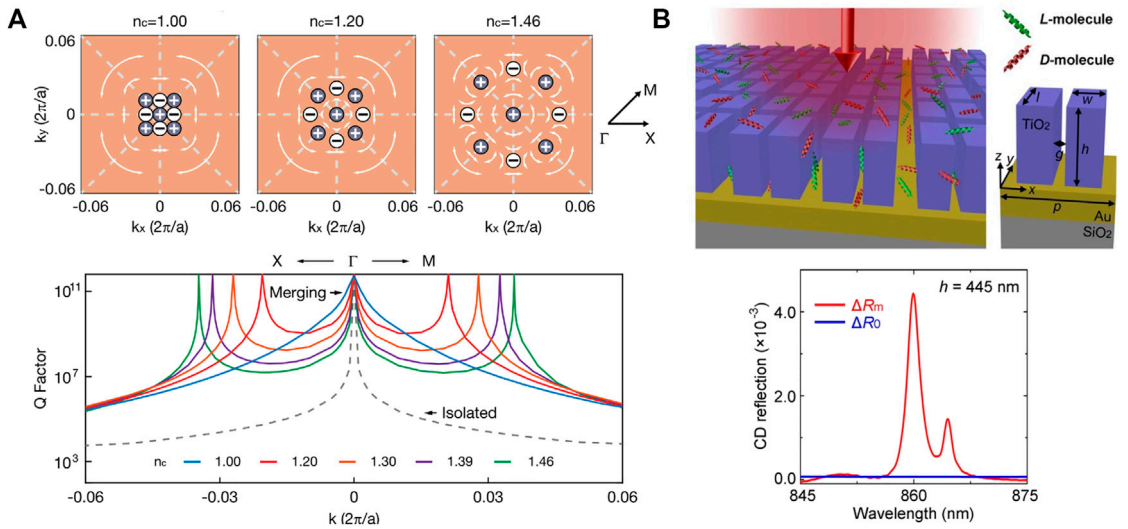

FIGURE 8 | Refractive index and chiral sensing applications. **(A)** Topological charge evolution of merging BICs and the Qs with refractive index variation [159], copyright IEEE. **(B)** Comparison of CD reflection spectrum of the BICs metasurface enhanced chiral layer and the bare chiral layer [160], copyright American Chemical Society.

"all-in-one" full Poincaré sphere polarizer. In addition, Yu et al. [143] reported a dynamic control of polarization conversion depending on the metasurfaces with electrically tunable refractive indices for the metasurface antennas.

Recently, 2D PhC slab structures were employed to manipulate the polarization without tuning the structural parameters [52, 146]. In particular, Guo et al. [52] achieved complete polarization conversion between linear polarizations, indicating the full energy exchange between *p*- and *s*-polarized incident lights; in addition, they proved such polarization conversion was topologically protected owing to the winding vector of the complex reflection coefficient. Complete polarization conversion happened at the vortex center, where a nonzero winding number (+1 or −1) in momentum space gave rise to a zero reflection coefficient, which is shown in **Figure 7C**. More interestingly, they revealed the relationship between the complete polarization conversion and the integer topological charges, namely the BICs. Given that the BICs correspond to the vanishing points of out-going coupling coefficients, they always appeared on the curves that supported complete polarization conversion in momentum space, thus bridging the phenomena with topological singularities.

Furthermore, arbitrary polarization conversion was proposed in a lossless 2D PhC slab [146]. Namely, by tuning the incident light with any given polarization towards a given direction that fell into a wide range of frequency, the polarization of the reflected light could cover the whole Poincaré sphere. **Figure 7D** shows the result of the reflected polarization under *s*-polarized incidence for frequency $0.402 \times 2\pi c/a$ and $0.405 \times 2\pi c/a$, in which a is the lattice constant. Complete polarization conversion occurred at W point where all the *s*-polarized incidence converted to *p*-polarized, related with the topological property of the scattering matrix [52]. Moreover, with losses, the 2D PhC slab system could still generate arbitrary output polarization if the input was *p*- or *s*-polarized.

3.6 Spectral and Chiral Sensing

Given that topological polarization singularities possess exotic characteristics upon the radiation fields, it is reasonable to utilize them for sensing the surrounding environment. In particular, the high-*Q* nature of integer charges (BICs), and the chiral responses of half charges (CPs) are two promising features. In a perturbated environment, the ideal BICs transform to quasi-BICs with shifted resonance wavelengths while remaining considerably high *Q*s, thus providing the capability of sensing small refractive-index changes from spectral observation. High sensitivity refractive index (RI) sensing in chemical and biological processes has been realized in many high-*Q* resonators [147–157]. The RI sensors based on BICs realized by dielectric metasurfaces and PhC slabs have also shown promising performances in figure-of-merit (FOM) and detection-limit (DL) [158, 159]. On the other hand, since chiral responses observed from the reflected or transmitted light can be used to distinguish the chirality of targets, chiral sensing were realized accordingly [160]. In addition, although not directly utilizing the polarization singularities, it is noteworthy to mention a class of novel methods that use the EPs to improve sensing performance [161–170], given by the underlying connections to the polarization singularities.

For instance, in 2017, Liu et al. [158] experimentally demonstrated RI sensing in a wavelength range of 1,400, –, 1,600 *nm* by applying the BICs in PhCs, which showed great potential for label-free optical biosensors. To further promote the sensing performance, it was important to suppress the out-of-

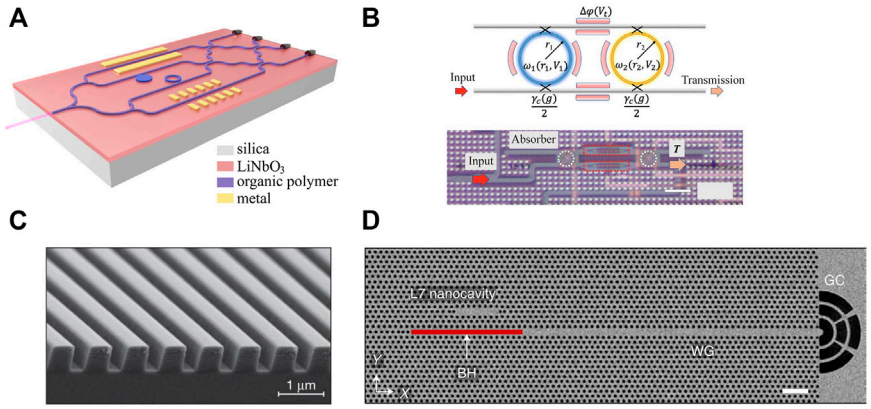

FIGURE 9 | BIC-based photonic integrated components, including **(A)** photonic circuit where low-refractive index material was patterned on a high-refractive-index substrate. Adapted with permission from [178] copyright The Optical Society, **(B)** filter [179], copyright American Physical Society. **(C)** Grating coupler [43], copyright Springer Nature Ltd. and **(D)** laser [180], copyright Springer Nature Ltd.

plane scattering loss caused by fabrication imperfections to improve the *Q*s. Following this strategic, Lv et al. [159] adopted the merging BIC design to RI sensing, which significantly promoted the DL performances in practice owing to the higher *Q*s (**Figure 8A**). However, the sensitivity of RI sensors are also related to the field overlap between the optical resonances and the targets embedded in surrounding environment. Methods such as breaking the in-plane symmetry or using low-contrast materials have been developed on PhC slabs [171] and metasurfaces [172] platforms for high-sensitivity hyper-spectral bio-molecular detection.

On the other hand, chiral sensing is desired in medical and biological applications. Since many biochemical compounds are chiral in nature, circular dichroism (CD) spectroscopy is utilized for the enantiomer-specific analysis of chiral samples. It is noteworthy that certain resonant nanostructures can significantly enhance the circular dichroism responses and improve the sensitivity of spectroscopy as well as photochemical, and thus ehannce the sensitivity of chiral sensing [173]. In 2019, Koshelev et al. [174] investigated the effect of detuning between the electrical and magnetic dipole resonances in silicon nano-cylinders in which the optical chirality at the nanoscale could be greatly enhanced. Later in 2020, Chen et al. [160] demonstrated the acquisition of CD spectrum and molar concentration over an individual metasurface with a high sensitivity (**Figure 8B**). Owing to the high-*Q* resonances, a hyperchiral field enhancement of the CD signal by a factor of 59 was observed, together with a large FOM of 80.6 in the detection of molar concentration, and thus it became a promising mythology in food industry, medical diagnostics, and drug development.

The EPs belong to a type of topologically non-trivial diabolic points. In 2017, for the first time, Chen et al. [170] proposed the scheme of using the micro-cavities operated at non-Hermitian spectral degeneracies for sensing. Owing to the complex-square-root dependency near an EP, the frequency splitting scaled as the square root of the perturbation strength, and hence, led to larger responses from small perturbation than that from traditional dispersion relations. This method paved the way for the sensors with unprecedented sensitivity. It is noteworthy that as mentioned in **Section 2.1**, the EPs are accompanied with polarization singularities, namely half-charges. Although not reported yet, we are optimistic to see the polarization singularity raised from EPs being utilized for sensing in the future.

3.7 Photonic Integration

Topological polarization singularities provide a vivid picture for light manipulation, which is useful in eliminating radiations, suppressing scatterings, and creating directional emitting, and thus shed light on the possibilities of photonic integration. Specifically, the superior photon confinement ability of the BICs leads to the ultra-high *Q*, ultra-narrow linewidth and low propagation loss, and the merging of half charges upon a single-side may boost the applications requiring unidirectional emission. Hereby we introduce some devices as examples, including waveguides [175–178], filters [179], couplers [43] and lasers [180].

By using BICs to confine light vertically, Zhang et al. [176] and Lin et al. [177] demonstrated waveguiding in PhC slabs. These works demonstrated the possibility to manipulate the radiation lifetime and spatial dispersion of BIC in a cooperative way. The BIC-based in-plane waveguiding was also utilized in the topological edge state in Zhang et al.'s work [175].

Recently, a new photonic platform with a low-refractive index material (Polymer) patterned on a high-refractive-index substrate ($LiNbO_3$) was demonstrated for integrated BIC-based devices including waveguides, microcavities, directional couplers, and modulators [178, 181]. This platform overcame the challenge of fabricating nano-scale structures upon high-refractive-index dielectric materials. The schematic of the platform in [178] is shown in **Figure 9A**. Specifically, the waveguide width was optimized and a BIC was observed by tuning the coupling strength between the TM bound mode and TE continuous mode. Benefiting from the BIC, the propagation loss of a straight waveguide was reduced to almost zero. For bent

waveguides, the bending loss was suppressed in a similar way by changing the bend radius and waveguide width. Besides, the BICs also provided an ultra-high Q, showing an intrinsic Q over 10^6 in microdisk cavities.

Gong et al. [179] implemented a BIC filter based on silicon photonic integrated circuits (PICs). The BIC filter was composed of two cascaded ring resonators side-coupled to two bus waveguides, as illuatrated in **Figure 9B**, with the two resonance frequencies $\omega_1$and ω_2 both tunable. By tuning the phase delay between the two rings to a multiple of π, the working state approached a near-FP-BIC [37] point, resulting in a filter performance with a near-unity transmission at $\omega_0 = \frac{\omega_1+\omega_2}{2}$ and a near-zero transmission at ω_1 and ω_2.

On the other hand, unidirectional guided resonances (UGRs) proposed by Yin et al. [43] paves the way to energy-efficient grating couplers. The UGRs only radiate toward one side of the PhC slab with the radiation at the other side eliminated (**Figure 9C**). The asymmetry ratio of the directional radiation reached 27.7 *dB* which indicated 99.8% of the power radiated toward the target direction. Moreover, the effect was maintained within a reasonably broad bandwidth (over 90% within a 26 *nm* bandwidth), and was proved to be effective for a coupling angle ranging from 5 to 11°.

The ultra-narrow linewidth of the BICs also facilitates the on-chip integrated lasers. Yu et al. experimentally an demonstrated a Fano BIC laser with a 5.8 *MHz* linewidth based on InP PhC slab buried within Si wafer [180](**Figure 9D**). Fano interference occurred between the discrete mode of a nanocavity and the continuum modes of a waveguide. The propagating modes in the waveguide destructively interfered with the nanocavity mode at the BIC wavelength, thereby turning the ordinary leaky mode into a BIC. Assuming an ideal BIC, a Fano mirror with total reflection would be formed in the waveguide region. Therefore, the light would be confined in the nanocavity and the region within the Fano mirror. The Q of the Fano BIC was significantly increased because photons were generated in the active region but stored in the passive region. Furthermore, the long lifetimes of the photons in the passive area can offset part of the quantum fluctuations caused by spontaneous radiation in the active area. The Fano BIC laser showed good mode selectivity and its lasing linewidth met the requirement of coherent optical communication.

4 DISCUSSION

In previous sections, we have reviewed the fundamentals and applications of polarization singularities that are defined upon the far-field radiations. As elaborated, the polarization singularities are topological in nature, with their existence and continuous evolution robust in the momentum space. From the view of science, polarization singularities reflect the "inside information" of a system which becomes observable since the escaping photons carry it out. On the other hand, polarization singularities establish abstract and primitive concepts for depicting, and further manipulating lights, and then pave the way to many applications as discussed.

For an outlook, several points might be noteworthy. From theoretical point of view, it is essential to build up a comprehensive connection between radiation topology, where polarization singularities are defined, and non-Hermitian topology, where generic topological band theory is developed upon. Given that radiation raises non-Hermiticity, it is expected that non-trivial intrinsic band topology might lead to observable manifestation in radiation field, that bridges to polarization singularities. Given that many exotic phenomena were discovered in non-Hermitian systems, it is necessary to study how the radiation raises and represents unique topology landscapes for deeper understanding of the physics. For instance, both the BICs and EPs carry topological charges in their far-field radiation, but only the latter are associated with nontrivial Chern numbers. Besides, from the view of technology, there's still much to explore about extending the idea of polarization singularity manipulation to more materials, devices, scenarios and applications. We are optimistic to foresee that the utilization of polarization singularities will be boosted by the methodology of topological photonics, thus bring essential promotion to many key applications, including optical communication, LIDAR, AR/VR, and bio-sensing.

AUTHOR CONTRIBUTIONS

CP organized the article. FW, CP, and XY composed Section 1, 2, and 4. All the authors contributed to Section 3.

FUNDING

This work was supported by the National Natural Science Foundation of China (Grant Nos. 61922004 and 62135001), China Postdoctoral Science Foundation funded project (Grant No. 2021M690239), National Key Research and Development Program of China (2020YFB1806405), and Major Key Project of PCL (PCL2021A14, PCL2021A04).

REFERENCES

1. Poincaré H. *Théorie mathématique de la lumière: cours de Physique Mathématique*. Paris: Georges Carré Editeur (1889).
2. Soskin MS, Vasnetsov MV. Singular Optics. *Prog Opt* (2001) 42:219–76. doi:10.1016/S0079-6638(01)80018-4
3. Nye JF. Lines of Circular Polarization in Electromagnetic Wave fields. *Proc R Soc Lond A* (1983) 389:279–90. doi:10.1098/rspa.1983.0109
4. Nye JF. Polarization Effects in the Diffraction of Electromagnetic Waves: the Role of Disclinations. *Proc R Soc Lond A* (1983) 387:105–32. doi:10.1098/rspa.1983.0053
5. Berry MV. Geometry of Phase and Polarization Singularities Illustrated by Edge Diffraction and the Tides. In: MS Soskin MV Vasnetsov, editors. *Second International Conference on Singular Optics (Optical Vortices): Fundamentals and Applications*, 4403. Crimea: International Society for Optics and Photonics (2001). p. 1–12. doi:10.1117/12.428252

6. Dennis MR, O'Holleran K, Padgett MJ. Chapter 5 Singular Optics: Optical Vortices and Polarization Singularities. *Prog Opt* (2009) 53:293–363. doi:10.1016/S0079-6638(08)00205-9
7. Gbur GJ. *Singular Optics*. Boca Raton: CRC Press (2016).
8. Berry M. *A Half-century of Physical Asymptotics and Other Diversions: Selected Works by Michael Berry*. Singapore: World Scientific (2017).
9. Wang Q, Tu C-H, Li Y-N, Wang H-T. Polarization Singularities: Progress, Fundamental Physics, and Prospects. *APL Photon* (2021) 6:040901. doi:10.1063/5.0045261
10. Allen L, Barnett SM, Padgett MJ. *Optical Angular Momentum*. Boca Raton: CRC Press (2016).
11. Desyatnikov AS, Torner L, Kivshar YS. *Optical Vortices and Vortex Solitons* (2005). *arXiv preprint nlin/0501026*.
12. Wang B, Liu W, Zhao M, Wang J, Zhang Y, Chen A, et al. Generating Optical Vortex Beams by Momentum-Space Polarization Vortices Centred at Bound States in the Continuum. *Nat Photon* (2020) 14:623–8. doi:10.1038/s41566-020-0658-1
13. Tovar AA. Production and Propagation of Cylindrically Polarized Laguerre-Gaussian Laser Beams. *J Opt Soc Am A* (1998) 15:2705–11. doi:10.1364/JOSAA.15.002705
14. Youngworth KS, Brown TG. Focusing of High Numerical Aperture Cylindrical-Vector Beams. *Opt Express* (2000) 7:77–87. doi:10.1364/OE.7.000077
15. Zhan Q, Leger J. Focus Shaping Using Cylindrical Vector Beams. *Opt Express* (2002) 10:324–31. doi:10.1364/OE.10.000324
16. Dorn R, Quabis S, Leuchs G. Sharper Focus for a Radially Polarized Light Beam. *Phys Rev Lett* (2003) 91:233901. doi:10.1103/PhysRevLett.91.233901
17. Hsu CW, Zhen B, Lee J, Chua S-L, Johnson SG, Joannopoulos JD, et al. Observation of Trapped Light within the Radiation Continuum. *Nature* (2013) 499:188–91. doi:10.1038/nature12289
18. Koshelev K, Kruk S, Melik-Gaykazyan E, Choi J-H, Bogdanov A, Park H-G, et al. Subwavelength Dielectric Resonators for Nonlinear Nanophotonics. *Science* (2020) 367:288–92. doi:10.1126/science.aaz3985
19. Bulgakov EN, Sadreev AF. Bound States in the Continuum with High Orbital Angular Momentum in a Dielectric Rod with Periodically Modulated Permittivity. *Phys Rev A* (2017) 96:013841. doi:10.1103/PhysRevA.96.013841
20. Zhang Y, Chen A, Liu W, Hsu CW, Wang B, Guan F, et al. Observation of Polarization Vortices in Momentum Space. *Phys Rev Lett* (2018) 120:186103. doi:10.1103/PhysRevLett.120.186103
21. von Neuman J, Wigner E. Über merkwürdige diskrete eigenwerte. Uber das verhalten von eigenwerten bei adiabatischen prozessen. *Physikalische Z* (1929) 30:467–70.
22. Plotnik Y, Peleg O, Dreisow F, Heinrich M, Nolte S, Szameit A, et al. Experimental Observation of Optical Bound States in the Continuum. *Phys Rev Lett* (2011) 107:183901. doi:10.1103/PhysRevLett.107.183901
23. Yang Y, Peng C, Liang Y, Li Z, Noda S. Analytical Perspective for Bound States in the Continuum in Photonic crystal Slabs. *Phys Rev Lett* (2014) 113:037401. doi:10.1103/PhysRevLett.113.037401
24. Ni L, Wang Z, Peng C, Li Z. Tunable Optical Bound States in the Continuum beyond In-Plane Symmetry protection. *Phys Rev B* (2016) 94:245148. doi:10.1103/PhysRevB.94.245148
25. Zhen B, Hsu CW, Lu L, Stone AD, Soljačić M. Topological Nature of Optical Bound States in the Continuum. *Phys Rev Lett* (2014) 113:257401. doi:10.1103/PhysRevLett.113.257401
26. Zhou H, Peng C, Yoon Y, Hsu CW, Nelson KA, Fu L, et al. Observation of Bulk Fermi Arc and Polarization Half Charge from Paired Exceptional Points. *Science* (2018) 359:1009–12. doi:10.1126/science.aap9859
27. Lu L, Joannopoulos JD, Soljačić M. Topological Photonics. *Nat Photon* (2014) 8:821–9. doi:10.1038/nphoton.2014.248
28. Khanikaev AB, Shvets G. Two-dimensional Topological Photonics. *Nat Photon* (2017) 11:763–73. doi:10.1038/s41566-017-0048-5
29. Ozawa T, Price HM, Amo A, Goldman N, Hafezi M, Lu L, et al. Topological Photonics. *Rev Mod Phys* (2019) 91:015006. doi:10.1103/revmodphys.91.015006
30. Parto M, Liu YGN, Bahari B, Khajavikhan M, Christodoulides DN. Non-Hermitian and Topological Photonics: Optics at an Exceptional point. *Nanophotonics* (2020) 10:403–23. doi:10.1515/nanoph-2020-0434
31. Feng L, El-Ganainy R, Ge L. Non-Hermitian Photonics Based on Parity-Time Symmetry. *Nat Photon* (2017) 11:752–62. doi:10.1038/s41566-017-0031-1
32. El-Ganainy R, Makris KG, Khajavikhan M, Musslimani ZH, Rotter S, Christodoulides DN. Non-Hermitian Physics and PT Symmetry. *Nat Phys* (2018) 14:11–9. doi:10.1038/nphys4323
33. Ghatak A, Das T. New Topological Invariants in Non-hermitian Systems. *J Phys Condens Matter* (2019) 31:263001. doi:10.1088/1361-648x/ab11b3
34. Ashida Y, Gong Z, Ueda M. Non-Hermitian Physics. *Adv Phys* (2020) 69:249–435. doi:10.1080/00018732.2021.1876991
35. Yin X, Peng C. Manipulating Light Radiation from a Topological Perspective. *Photon Res* (2020) 8:B25. doi:10.1364/prj.403444
36. Peng C. Trapping Light in the Continuum - from Fantasy to Reality. *Sci Bull* (2020) 65:1527–32. doi:10.1016/j.scib.2020.05.009
37. Hsu CW, Zhen B, Stone AD, Joannopoulos JD, Soljačić M. Bound States in the Continuum. *Nat Rev Mater* (2016) 1:16048. doi:10.1038/natrevmats.2016.48
38. Koshelev K, Bogdanov A, Kivshar Y. Meta-optics and Bound States in the Continuum. *Sci Bull* (2019) 64:836–42. doi:10.1016/j.scib.2018.12.003
39. Azzam SI, Kildishev AV. Photonic Bound States in the Continuum: From Basics to Applications. *Adv Opt Mater*. (2021) 9:2001469. doi:10.1002/adom.202001469
40. Allen L, Padgett MJ, Babiker M. IV the Orbital Angular Momentum of Light. In: E Wolf, editor. *Progress in Optics*, 39. New York: Elsevier (1999). p. 291–372. doi:10.1016/S0079-6638(08)70391-3.ISSN:0079-6638
41. Franke-Arnold S, Allen L, Padgett M. Advances in Optical Angular Momentum. *Laser Photon Rev* (2008) 2:299–313. doi:10.1002/lpor.200810007
42. Padgett MJ. Orbital Angular Momentum 25 Years on [Invited]. *Opt Express* (2017) 25:11265. doi:10.1364/oe.25.011265
43. Yin X, Jin J, Soljačić M, Peng C, Zhen B. Observation of Topologically Enabled Unidirectional Guided Resonances. *Nature* (2020) 580:467–71. doi:10.1038/s41586-020-2181-4
44. Kravets VG, Schedin F, Jalil R, Britnell L, Gorbachev RV, Ansell D, et al. Singular Phase Nano-Optics in Plasmonic Metamaterials for Label-free Single-Molecule Detection. *Nat Mater* (2013) 12:304–9. doi:10.1038/nmat3537
45. Ramezani H, Li H-K, Wang Y, Zhang X. Unidirectional Spectral Singularities. *Phys Rev Lett* (2014) 113:263905. doi:10.1103/PhysRevLett.113.263905
46. Sreekanth KV, Sreejith S, Han S, Mishra A, Chen X, Sun H, et al. Biosensing with the Singular Phase of an Ultrathin Metal-Dielectric Nanophotonic Cavity. *Nat Commun* (2018) 9:369. doi:10.1038/s41467-018-02860-6
47. Li Y, Argyropoulos C. Exceptional Points and Spectral Singularities in Active Epsilon-Near-Zero Plasmonic Waveguides. *Phys Rev B* (2019) 99:075413. doi:10.1103/PhysRevB.99.075413
48. Shen Y, Wang X, Xie Z, Min C, Fu X, Liu Q, et al. Optical Vortices 30 Years on: OAM Manipulation from Topological Charge to Multiple Singularities. *Light Sci Appl* (2019) 8:90. doi:10.1038/s41377-019-0194-2
49. Han Z, Ohno S, Minamide H. Spectral Phase Singularity in a Transmission-type Double-Layer Metamaterial. *Optica* (2020) 7:1721. doi:10.1364/OPTICA.404090
50. Ni J, Huang C, Zhou L-M, Gu M, Song Q, Kivshar Y, et al. Multidimensional Phase Singularities in Nanophotonics. *Science* (2021) 374:eabj0039. doi:10.1126/science.abj0039
51. Liu M, Zhao C, Zeng Y, Chen Y, Zhao C, Qiu C-W. Evolution and Nonreciprocity of Loss-Induced Topological Phase Singularity Pairs. *Phys Rev Lett* (2021) 127:266101. doi:10.1103/PhysRevLett.127.266101
52. Guo Y, Xiao M, Fan S. Topologically Protected Complete Polarization Conversion. *Phys Rev Lett* (2017) 119:167401. doi:10.1103/PhysRevLett.119.167401
53. Dai S, Liu L, Han D, Zi J. From Topologically Protected Coherent Perfect Reflection to Bound States in the Continuum. *Phys Rev B* (2018) 98:081405. doi:10.1103/PhysRevB.98.081405
54. Sweeney WR, Hsu CW, Stone AD. Theory of Reflectionless Scattering Modes. *Phys Rev A* (2020) 102:063511. doi:10.1103/PhysRevA.102.063511
55. Wong WC, Wang W, Yau WT, Fung KH. Topological Theory for Perfect Metasurface Isolators. *Phys Rev B* (2020) 101:121405. doi:10.1103/PhysRevB.101.121405
56. Mukherjee S, Gomis-Bresco J, Pujol-Closa P, Artigas D, Torner L. Topological Properties of Bound States in the Continuum in Geometries

with Broken Anisotropy Symmetry. *Phys Rev A* (2018) 98:063826. doi:10.1103/PhysRevA.98.063826
57. Song AY, Catrysse PB, Fan S. Broadband Control of Topological Nodes in Electromagnetic fields. *Phys Rev Lett* (2018) 120:193903. doi:10.1103/PhysRevLett.120.193903
58. Xiao Y-X, Ding K, Zhang R-Y, Hang ZH, Chan CT. Exceptional Points Make an Astroid in Non-hermitian Lieb Lattice: Evolution and Topological protection. *Phys Rev B* (2020) 102:245144. doi:10.1103/PhysRevB.102.245144
59. Tong H, Liu S, Zhao M, Fang K. Observation of Phonon Trapping in the Continuum with Topological Charges. *Nat Commun* (2020) 11:5216. doi:10.1038/s41467-020-19091-3
60. Ilic O, Kaminer I, Zhen B, Miller OD, Buljan H, Soljačić M. Topologically Enabled Optical Nanomotors. *Sci Adv* (2017) 3:9. doi:10.1126/sciadv.1602738
61. Friedrich H, Wintgen D. Interfering Resonances and Bound States in the Continuum. *Phys Rev A* (1985) 32:3231–42. doi:10.1103/physreva.32.3231
62. Huang MCY, Zhou Y, Chang-Hasnain CJ. A Surface-Emitting Laser Incorporating a high-index-contrast Subwavelength Grating. *Nat Photon* (2007) 1:119–22. doi:10.1038/nphoton.2006.80
63. Zhou Y, Huang MCY, Chang-Hasnain CJ. Large Fabrication Tolerance for VCSELs Using High-Contrast Grating. *IEEE Photon Technol Lett* (2008) 20:434–6. doi:10.1109/LPT.2008.916969
64. Huang MCY, Zhou Y, Chang-Hasnain CJ. Single Mode High-Contrast Subwavelength Grating Vertical Cavity Surface Emitting Lasers. *Appl Phys Lett* (2008) 92:171108. doi:10.1063/1.2917447
65. Ye Zhou Y, Huang MCY, Chase C, Karagodsky V, Moewe M, Pesala B, et al. High-index-contrast Grating (HCG) and its Applications in Optoelectronic Devices. *IEEE J Select Top Quan Electron.* (2009) 15:1485–99. doi:10.1109/JSTQE.2009.2021145
66. Wang Z, Zhang H, Ni L, Hu W, Peng C. Analytical Perspective of Interfering Resonances in high-index-contrast Periodic Photonic Structures. *IEEE J Quan Electron.* (2016) 52:1–9. doi:10.1109/JQE.2016.2568763
67. Lee S-G, Magnusson R. Band Flips and Bound-State Transitions in Leaky-Mode Photonic Lattices. *Phys Rev B* (2019) 99:045304. doi:10.1103/PhysRevB.99.045304
68. Koshelev K, Lepeshov S, Liu M, Bogdanov A, Kivshar Y. Asymmetric Metasurfaces with High- Q Resonances Governed by Bound States in the Continuum. *Phys Rev Lett* (2018) 121:193903. doi:10.1103/PhysRevLett.121.193903
69. Liu Z, Xu Y, Lin Y, Xiang J, Feng T, Cao Q, et al. High- Q Quasibound States in the Continuum for Nonlinear Metasurfaces. *Phys Rev Lett* (2019) 123:253901. doi:10.1103/PhysRevLett.123.253901
70. Yesilkoy F, Arvelo ER, Jahani Y, Liu M, Tittl A, Cevher V, et al. Ultrasensitive Hyperspectral Imaging and Biodetection Enabled by Dielectric Metasurfaces. *Nat Photon* (2019) 13:390–6. doi:10.1038/s41566-019-0394-6
71. Chen A, Liu W, Zhang Y, Wang B, Liu X, Shi L, et al. Observing Vortex Polarization Singularities at Optical Band Degeneracies. *Phys Rev B* (2019) 99:180101. doi:10.1103/PhysRevB.99.180101
72. Chen W, Chen Y, Liu W. Line Singularities and Hopf Indices of Electromagnetic Multipoles. *Laser Photon Rev* (2020) 14:2000049. doi:10.1002/lpor.202000049
73. Chen W, Chen Y, Liu W. Singularities and Poincaré Indices of Electromagnetic Multipoles. *Phys Rev Lett* (2019) 122:153907. doi:10.1103/PhysRevLett.122.153907
74. Sadrieva Z, Frizyuk K, Petrov M, Kivshar Y, Bogdanov A. Multipolar Origin of Bound States in the Continuum. *Phys Rev B* (2019) 100:115303. doi:10.1103/PhysRevB.100.115303
75. Streifer W, Scifres D, Burnham R. Analysis of Grating-Coupled Radiation in GaAs:GaAlAs Lasers and Waveguides - I. *IEEE J Quan Electron.* (1976) 12:422–8. doi:10.1109/JQE.1976.1069175
76. Kim M, Kim CS, Bewley WW, Lindle JR, Canedy CL, Vurgaftman I, et al. Surface-emitting Photonic-crystal Distributed-Feedback Laser for the Midinfrared. *Appl Phys Lett* (2006) 88:191105. doi:10.1063/1.2203234
77. Lu T-C, Chen S-W, Lin L-F, Kao T-T, Kao C-C, Yu P, et al. GaN-based Two-Dimensional Surface-Emitting Photonic crystal Lasers with AlN/GaN Distributed Bragg Reflector. *Appl Phys Lett* (2008) 92:011129. doi:10.1063/1.2831716
78. Matsubara H, Yoshimoto S, Saito H, Jianglin Y, Tanaka Y, Noda S. GaN Photonic-crystal Surface-Emitting Laser at Blue-Violet Wavelengths. *Science* (2008) 319:445–7. doi:10.1126/science.1150413
79. Chassagneux Y, Colombelli R, Maineult W, Barbieri S, Beere HE, Ritchie DA, et al. Electrically Pumped Photonic-crystal Terahertz Lasers Controlled by Boundary Conditions. *Nature* (2009) 457:174–8. doi:10.1038/nature07636
80. Imada M, Noda S, Chutinan A, Tokuda T, Murata M, Sasaki G. Coherent Two-Dimensional Lasing Action in Surface-Emitting Laser with Triangular-Lattice Photonic crystal Structure. *Appl Phys Lett* (1999) 75:316–8. doi:10.1063/1.124361
81. Ohnishi D, Okano T, Imada M, Noda S. Room Temperature Continuous Wave Operation of a Surface-Emitting Two-Dimensional Photonic crystal Diode Laser. *Opt Express* (2004) 12:1562. doi:10.1364/OPEX.12.001562
82. Hirose K, Liang Y, Kurosaka Y, Watanabe A, Sugiyama T, Noda S. Watt-class High-Power, High-Beam-Quality Photonic-crystal Lasers. *Nat Photon* (2014) 8:406–11. doi:10.1038/nphoton.2014.75
83. Yoshida M, De Zoysa M, Ishizaki K, Tanaka Y, Kawasaki M, Hatsuda R, et al. Double-lattice Photonic-crystal Resonators Enabling High-Brightness Semiconductor Lasers with Symmetric Narrow-Divergence Beams. *Nat Mater* (2019) 18:121–8. doi:10.1038/s41563-018-0242-y
84. Kodigala A, Lepetit T, Gu Q, Bahari B, Fainman Y, Kanté B. Lasing Action from Photonic Bound States in Continuum. *Nature* (2017) 541:196–9. doi:10.1038/nature20799
85. Bulgakov EN, Maksimov DN. Topological Bound States in the Continuum in Arrays of Dielectric Spheres. *Phys Rev Lett* (2017) 118:267401. doi:10.1103/PhysRevLett.118.267401
86. Doeleman HM, Monticone F, den Hollander W, Alù A, Koenderink AF. Experimental Observation of a Polarization Vortex at an Optical Bound State in the Continuum. *Nat Photon* (2018) 12:397–401. doi:10.1038/s41566-018-0177-5
87. Wang Z, Liang Y, Beck M, Scalari G, Faist J. Topological Charge of Finite-Size Photonic crystal Modes. *Phys Rev B* (2020) 102:045122. doi:10.1103/PhysRevB.102.045122
88. Bulgakov EN, Pichugin KN, Sadreev AF. All-optical Light Storage in Bound States in the Continuum and Release by Demand. *Opt Express* (2015) 23:22520. doi:10.1364/OE.23.022520
89. Bulgakov EN, Maksimov DN. Bound States in the Continuum and Polarization Singularities in Periodic Arrays of Dielectric Rods. *Phys Rev A* (2017) 96:063833. doi:10.1103/PhysRevA.96.063833
90. Bulgakov EN, Sadreev AF. Light Trapping above the Light Cone in a One-Dimensional Array of Dielectric Spheres. *Phys Rev A* (2015) 92:023816. doi:10.1103/PhysRevA.92.023816
91. Carletti L, Koshelev K, De Angelis C, Kivshar Y. Giant Nonlinear Response at the Nanoscale Driven by Bound States in the Continuum. *Phys Rev Lett* (2018) 121:033903. doi:10.1103/PhysRevLett.121.033903
92. Rybin MV, Koshelev KL, Sadrieva ZF, Samusev KB, Bogdanov AA, Limonov MF, et al. High- Q Supercavity Modes in Subwavelength Dielectric Resonators. *Phys Rev Lett* (2017) 119:243901. doi:10.1103/PhysRevLett.119.243901
93. Silveirinha MG. Trapping Light in Open Plasmonic Nanostructures. *Phys Rev A* (2014) 89:023813. doi:10.1103/physreva.89.023813
94. Yoda T, Notomi M. Generation and Annihilation of Topologically Protected Bound States in the Continuum and Circularly Polarized States by Symmetry Breaking. *Phys Rev Lett* (2020) 125:053902. doi:10.1103/PhysRevLett.125.053902
95. Cerjan A, Hsu CW, Rechtsman MC. Bound States in the Continuum through Environmental Design. *Phys Rev Lett* (2019) 123:023902. doi:10.1103/PhysRevLett.123.023902
96. Cerjan A, Jörg C, Vaidya S, Augustine S, Benalcazar WA, Hsu CW, et al. Observation of Bound States in the Continuum Embedded in Symmetry Bandgaps. *Sci Adv* (2021) 7:eabk1117. doi:10.1126/sciadv.abk1117
97. De Angelis L, Bauer T, Alpeggiani F, Kuipers L. Index-symmetry Breaking of Polarization Vortices in 2D Random Vector Waves. *Optica* (2019) 6:1237. doi:10.1364/OPTICA.6.001237
98. Che Z, Zhang Y, Liu W, Zhao M, Wang J, Zhang W, et al. Polarization Singularities of Photonic Quasicrystals in Momentum Space. *Phys Rev Lett* (2021) 127:043901. doi:10.1103/PhysRevLett.127.043901
99. Song Q, Hu J, Dai S, Zheng C, Han D, Zi J, et al. Coexistence of a New Type of Bound State in the Continuum and a Lasing Threshold Mode Induced by Pt Symmetry. *Sci Adv* (2020) 6:eabc1160. doi:10.1126/sciadv.abc1160
100. Liu W, Wang B, Zhang Y, Wang J, Zhao M, Guan F, et al. Circularly Polarized States Spawning from Bound States in the Continuum. *Phys Rev Lett* (2019) 123:116104. doi:10.1103/PhysRevLett.123.116104

101. Ye W, Gao Y, Liu J. Singular Points of Polarizations in the Momentum Space of Photonic crystal Slabs. *Phys Rev Lett* (2020) 124:153904. doi:10.1103/PhysRevLett.124.153904
102. Zeng Y, Hu G, Liu K, Tang Z, Qiu C-W. Dynamics of Topological Polarization Singularity in Momentum Space. *Phys Rev Lett* (2021) 127:176101. doi:10.1103/PhysRevLett.127.176101
103. Chen W, Yang Q, Chen Y, Liu W. Evolution and Global Charge Conservation for Polarization Singularities Emerging from Non-hermitian Degeneracies. *Proc Natl Acad Sci USA* (2021) 118:e2019578118. doi:10.1073/pnas.2019578118
104. Jin J, Yin X, Ni L, Soljačić M, Zhen B, Peng C. Topologically Enabled Ultrahigh-Q Guided Resonances Robust to Out-Of-Plane Scattering. *Nature* (2019) 574:501–4. doi:10.1038/s41586-019-1664-7
105. Kang M, Zhang S, Xiao M, Xu H. Merging Bound States in the Continuum at Off-High Symmetry Points. *Phys Rev Lett* (2021) 126:117402. doi:10.1103/PhysRevLett.126.117402
106. Lee J, Zhen B, Chua S-L, Qiu W, Joannopoulos JD, Soljačić M, et al. Observation and Differentiation of Unique High-QOptical Resonances Near Zero Wave Vector in Macroscopic Photonic Crystal Slabs. *Phys Rev Lett* (2012) 109:067401. doi:10.1103/PhysRevLett.109.067401
107. Chen Z, Yin X, Jin J, Zheng Z, Zhang Z, Wang F, et al. Observation of Miniaturized Bound States in the Continuum with Ultra-high Quality Factors. *Sci Bull* (2022) 67:359–66. doi:10.1016/j.scib.2021.10.020
108. Akahane Y, Asano T, Song B-S, Noda S. High-*Q* Photonic Nanocavity in a Two-Dimensional Photonic crystal. *Nature* (2003) 425:944–7. doi:10.1038/nature02063
109. Song B-S, Noda S, Asano T, Akahane Y. Ultra-high-*Q* Photonic Double-Heterostructure Nanocavity. *Nat Mater* (2005) 4:207–10. doi:10.1038/nmat1320
110. Deotare PB, McCutcheon MW, Frank IW, Khan M, Lončar M. High Quality Factor Photonic crystal Nanobeam Cavities. *Appl Phys Lett* (2009) 94:121106. doi:10.1063/1.3107263
111. Chua S-L, Chong Y, Stone AD, Soljacic M, Bravo-Abad J. Low-threshold Lasing Action in Photonic crystal Slabs Enabled by Fano Resonances. *Opt Express* (2011) 19:1539. doi:10.1364/OE.19.001539
112. Liang Y, Peng C, Sakai K, Iwahashi S, Noda S. Three-dimensional Coupled-Wave Analysis for Square-Lattice Photonic crystal Surface Emitting Lasers with Transverse-Electric Polarization: Finite-Size Effects. *Opt Express* (2012) 20:15945. doi:10.1364/OE.20.015945
113. Hwang M-S, Lee H-C, Kim K-H, Jeong K-Y, Kwon S-H, Koshelev K, et al. Ultralow-threshold Laser Using Super-bound States in the Continuum. *Nat Commun* (2021) 12:4135. doi:10.1038/s41467-021-24502-0
114. Wang J, Clementi M, Minkov M, Barone A, Carlin J-F, Grandjean N, et al. Doubly Resonant Second-Harmonic Generation of a Vortex Beam from a Bound State in the Continuum. *Optica* (2020) 7:1126. doi:10.1364/OPTICA.396408
115. Shyh Wang S. Principles of Distributed Feedback and Distributed Bragg-Reflector Lasers. *IEEE J Quan Electron.* (1974) 10:413–27. doi:10.1109/jqe.1974.1068152
116. Reinhart FK, Logan RA, Shank CV. GaAs-AlxGa1-xAs Injection Lasers with Distributed Bragg Reflectors. *Appl Phys Lett* (1975) 27:45–8. doi:10.1063/1.88262
117. Hasnain G, Tai K, Yang L, Wang YH, Fischer RJ, Wynn JD, et al. Performance of Gain-Guided Surface Emitting Lasers with Semiconductor Distributed Bragg Reflectors. *IEEE J Quan Electron.* (1991) 27:1377–85. doi:10.1109/3.89954
118. Kurosaka Y, Iwahashi S, Liang Y, Sakai K, Miyai E, Kunishi W, et al. On-chip Beam-Steering Photonic-crystal Lasers. *Nat Photon* (2010) 4:447–50. doi:10.1038/nphoton.2010.118
119. Peng C, Liang Y, Sakai K, Iwahashi S, Noda S. Three-dimensional Coupled-Wave Theory Analysis of a Centered-Rectangular Lattice Photonic crystal Laser with a Transverse-electric-like Mode. *Phys Rev B* (2012) 86:035108. doi:10.1103/physrevb.86.035108
120. Ishizaki K, Zoysa MD, Noda S. Progress in Photonic-crystal Surface-Emitting Lasers. *Photonics* (2019) 6:96. doi:10.3390/photonics6030096
121. Miyai E, Sakai K, Okano T, Kunishi W, Ohnishi D, Noda S. Lasers Producing Tailored Beams. *Nature* (2006) 441:946. doi:10.1038/441946a
122. Morita R, Inoue T, De Zoysa M, Ishizaki K, Noda S. Photonic-crystal Lasers with Two-Dimensionally Arranged Gain and Loss Sections for High-Peak-Power Short-Pulse Operation. *Nat Photon* (2021) 15:311–8. doi:10.1038/s41566-021-00771-5
123. Sakata R, Ishizaki K, De Zoysa M, Fukuhara S, Inoue T, Tanaka Y, et al. Dually Modulated Photonic Crystals Enabling High-Power High-Beam-Quality Two-Dimensional Beam Scanning Lasers. *Nat Commun* (2020) 11:3487. doi:10.1038/s41467-020-17092-w
124. Huang C, Zhang C, Xiao S, Wang Y, Fan Y, Liu Y, et al. Ultrafast Control of Vortex Microlasers. *Science* (2020) 367:1018–21. doi:10.1126/science.aba4597
125. Ha ST, Fu YH, Emani NK, Pan Z, Bakker RM, Paniagua-Domínguez R, et al. Directional Lasing in Resonant Semiconductor Nanoantenna Arrays. *Nat Nanotech* (2018) 13:1042–7. doi:10.1038/s41565-018-0245-5
126. Wu M, Ha ST, Shendre S, Durmusoglu EG, Koh W-K, Abujetas DR, et al. Room-Temperature Lasing in Colloidal Nanoplatelets via Mie-Resonant Bound States in the Continuum. *Nano Lett* (2020) 20:6005–11. doi:10.1021/acs.nanolett.0c01975
127. Xu L, Zangeneh Kamali K, Huang L, Rahmani M, Smirnov A, Camacho-Morales R, et al. Dynamic Nonlinear Image Tuning through Magnetic Dipole Quasi-BIC Ultrathin Resonators. *Adv Sci* (2019) 6:1802119. doi:10.1002/advs.201802119
128. Kang L, Wu Y, Ma X, Lan S, Werner DH. High-Harmonic Optical Vortex Generation from Photonic Bound States in the Continuum. *Adv Opt Mater* (2021) 10:2101497. doi:10.1002/adom.202101497
129. Wang J, Li H, Ma Y, Zhao M, Liu W, Wang B, et al. Routing valley Exciton Emission of a WS2 Monolayer via Delocalized Bloch Modes of In-Plane Inversion-Symmetry-Broken Photonic crystal Slabs. *Light Sci Appl* (2020) 9:148. doi:10.1038/s41377-020-00387-4
130. Koshelev K, Tang Y, Li K, Choi D-Y, Li G, Kivshar Y. Nonlinear Metasurfaces Governed by Bound States in the Continuum. *ACS Photon* (2019) 6:1639–44. doi:10.1021/acsphotonics.9b00700
131. Koshelev KL, Sychev SK, Sadrieva ZF, Bogdanov AA, Iorsh IV. Strong Coupling between Excitons in Transition Metal Dichalcogenides and Optical Bound States in the Continuum. *Phys Rev B* (2018) 98:161113. doi:10.1103/PhysRevB.98.161113
132. Kravtsov V, Khestanova E, Benimetskiy FA, Ivanova T, Samusev AK, Sinev IS, et al. Nonlinear Polaritons in a Monolayer Semiconductor Coupled to Optical Bound States in the Continuum. *Light Sci Appl* (2020) 9:56. doi:10.1038/s41377-020-0286-z
133. Yu Z, Wang Y, Sun B, Tong Y, Xu JB, Tsang HK, et al. Hybrid 2D-Material Photonics with Bound States in the Continuum. *Adv Opt Mater.* (2019) 7:1901306. doi:10.1002/adom.201901306
134. Tian J, Li Q, Belov PA, Sinha RK, Qian W, Qiu M. High-Q All-Dielectric Metasurface: Super and Suppressed Optical Absorption. *ACS Photon* (2020) 7:1436–43. doi:10.1021/acsphotonics.0c00003
135. Zhang Z, Yin X, Chen Z, Wang F, Hu W, Peng C. Observation of Intensity Flattened Phase Shifting Enabled by Unidirectional Guided Resonance. *Nanophotonics* (2021) 10:4467–75. doi:10.1515/nanoph-2021-0393
136. Lv J, Yin X, Jin J, Zhang H, Zhao C, Peng C, et al. Demonstration of a Thermo-Optic Phase Shifter by Utilizing High-Q Resonance in high-index-contrast Grating. *Opt Lett* (2018) 43:827. doi:10.1364/OL.43.000827
137. Kwon H, Zheng T, Faraon A. Nano-electromechanical Tuning of Dual-Mode Resonant Dielectric Metasurfaces for Dynamic Amplitude and Phase Modulation. *Nano Lett* (2021) 21:2817–23. doi:10.1021/acs.nanolett.0c04888
138. Salary MM, Mosallaei H. Tunable All-Dielectric Metasurfaces for Phase-Only Modulation of Transmitted Light Based on Quasi-Bound States in the Continuum. *ACS Photon* (2020) 7:1813–29. doi:10.1021/acsphotonics.0c00554
139. Xiong W, Hsu CW, Bromberg Y, Antonio-Lopez JE, Amezcua Correa R, Cao H. Complete Polarization Control in Multimode Fibers with Polarization and Mode Coupling. *Light Sci Appl* (2018) 7:54. doi:10.1038/s41377-018-0047-4
140. Li G, Chen S, Pholchai N, Reineke B, Wong PWH, Pun EYB, et al. Continuous Control of the Nonlinearity Phase for Harmonic Generations. *Nat Mater* (2015) 14:607–12. doi:10.1038/nmat4267
141. Rubin NA, D'Aversa G, Chevalier P, Shi Z, Chen WT, Capasso F. Matrix Fourier Optics Enables a Compact Full-Stokes Polarization Camera. *Science* (2019) 365:eaax1839. doi:10.1126/science.aax1839
142. Khan MI, Khalid Z, Tahir FA. Linear and Circular-Polarization Conversion in X-Band Using Anisotropic Metasurface. *Sci Rep* (2019) 9:4552. doi:10.1038/s41598-019-40793-2

143. Yu P, Li J, Liu N. Electrically Tunable Optical Metasurfaces for Dynamic Polarization Conversion. *Nano Lett* (2021) 21:6690–5. doi:10.1021/acs.nanolett.1c02318
144. Chang C-C, Zhao Z, Li D, Taylor AJ, Fan S, Chen H-T. Broadband Linear-To-Circular Polarization Conversion Enabled by Birefringent Off-Resonance Reflective Metasurfaces. *Phys Rev Lett* (2019) 123:237401. doi:10.1103/PhysRevLett.123.237401
145. Wang S, Deng Z-L, Wang Y, Zhou Q, Wang X, Cao Y, et al. Arbitrary Polarization Conversion Dichroism Metasurfaces for All-In-One Full Poincaré Sphere Polarizers. *Light Sci Appl* (2021) 10:24. doi:10.1038/s41377-021-00468-y
146. Guo Y, Xiao M, Zhou Y, Fan S. Arbitrary Polarization Conversion with a Photonic crystal Slab. *Adv Opt Mater.* (2019) 7:1801453. doi:10.1002/adom.201801453
147. Dorfner D, Zabel T, Hürlimann T, Hauke N, Frandsen L, Rant U, et al. Photonic crystal Nanostructures for Optical Biosensing Applications. *Biosens Bioelectron* (2009) 24:3688–92. doi:10.1016/j.bios.2009.05.014
148. Huang M, Yanik AA, Chang T-Y, Altug H. Sub-wavelength Nanofluidics in Photonic crystal Sensors. *Opt Express* (2009) 17:24224–33. doi:10.1364/OE.17.024224
149. Kang C, Phare CT, Vlasov YA, Assefa S, Weiss SM. Photonic crystal Slab Sensor with Enhanced Surface Area. *Opt Express* (2010) 18:27930–7. doi:10.1364/OE.18.027930
150. Lai W-C, Chakravarty S, Zou Y, Guo Y, Chen RT. Slow Light Enhanced Sensitivity of Resonance Modes in Photonic crystal Biosensors. *Appl Phys Lett* (2013) 102:041111. doi:10.1063/1.4789857
151. Lee MR, Fauchet PM. Two-dimensional Silicon Photonic crystal Based Biosensing Platform for Protein Detection. *Opt Express* (2007) 15:4530–5. doi:10.1364/OE.15.004530
152. Nicolaou C, Lau WT, Gad R, Akhavan H, Schilling R, Levi O. Enhanced Detection Limit by Dark Mode Perturbation in 2D Photonic crystal Slab Refractive index Sensors. *Opt Express* (2013) 21:31698–712. doi:10.1364/OE.21.031698
153. Sun Y, Fan X. Analysis of Ring Resonators for Chemical Vapor Sensor Development. *Opt Express* (2008) 16:10254–68. doi:10.1364/OE.16.010254
154. Tu X, Chen S-L, Song C, Huang T, Guo LJ. Ultrahigh Q Polymer Microring Resonators for Biosensing Applications. *IEEE Photon J.* (2019) 11:1–10. doi:10.1109/jphot.2019.2899666
155. Vollmer F, Arnold S. Whispering-gallery-mode Biosensing: Label-free Detection Down to Single Molecules. *Nat Methods* (2008) 5:591–6. doi:10.1038/nmeth.1221
156. Wang S, Liu Y, Zhao D, Yang H, Zhou W, Sun Y. Optofluidic Fano Resonance Photonic crystal Refractometric Sensors. *Appl Phys Lett* (2017) 110:091105. doi:10.1063/1.4977563
157. Xiao Y-F, Zou C-L, Li B-B, Li Y, Dong C-H, Han Z-F, et al. High-QExterior Whispering-Gallery Modes in a Metal-Coated Microresonator. *Phys Rev Lett* (2010) 105:153902. doi:10.1103/PhysRevLett.105.153902
158. Liu Y, Zhou W, Sun Y. Optical Refractive Index Sensing Based on High-Q Bound States in the Continuum in Free-Space Coupled Photonic Crystal Slabs. *Sensors* (2017) 17:1861. doi:10.3390/s17081861
159. Lv J, Chen Z, Yin X, Zhang Z, Hu W, Peng C. High-sensitive Refractive index Sensing Enabled by Topological Charge Evolution. *IEEE Photon J.* (2020) 12:1–10. doi:10.1109/jphot.2020.3017806
160. Chen Y, Zhao C, Zhang Y, Qiu C-w. Integrated Molar Chiral Sensing Based on High-Q Metasurface. *Nano Lett* (2020) 20:8696–703. doi:10.1021/acs.nanolett.0c03506
161. Heiss WD. Repulsion of Resonance States and Exceptional Points. *Phys Rev E* (2000) 61:929–32. doi:10.1103/PhysRevE.61.929
162. Berry MV. Physics of Nonhermitian Degeneracies. *Czechoslovak J Phys* (2004) 54:1039–47. doi:10.1023/B:CJOP.0000044002.05657.04
163. Dembowski C, Gräf H-D, Harney HL, Heine A, Heiss WD, Rehfeld H, et al. Experimental Observation of the Topological Structure of Exceptional Points. *Phys Rev Lett* (2001) 86:787–90. doi:10.1103/PhysRevLett.86.787
164. Lee S-B, Yang J, Moon S, Lee S-Y, Shim J-B, Kim SW, et al. Observation of an Exceptional point in a Chaotic Optical Microcavity. *Phys Rev Lett* (2009) 103:134101. doi:10.1103/PhysRevLett.103.134101
165. Zhu J, Özdemir ŞK, He L, Yang L. Controlled Manipulation of Mode Splitting in an Optical Microcavity by Two Rayleigh Scatterers. *Opt Express* (2010) 18:23535–43. doi:10.1364/OE.18.023535
166. Peng B, Özdemir ŞK, Liertzer M, Chen W, Kramer J, Yılmaz H, et al. Chiral Modes and Directional Lasing at Exceptional Points. *Proc Natl Acad Sci USA* (2016) 113:6845–50. doi:10.1073/pnas.1603318113
167. Choi Y, Kang S, Lim S, Kim W, Kim J-R, Lee J-H, et al. Quasieigenstate Coalescence in an Atom-Cavity Quantum Composite. *Phys Rev Lett* (2010) 104:153601. doi:10.1103/PhysRevLett.104.153601
168. Zhen B, Hsu CW, Igarashi Y, Lu L, Kaminer I, Pick A, et al. Spawning Rings of Exceptional Points Out of Dirac Cones. *Nature* (2015) 525:354–8. doi:10.1038/nature14889
169. Gao T, Estrecho E, Bliokh KY, Liew TCH, Fraser MD, Brodbeck S, et al.Observation of Non-hermitian Degeneracies in a Chaotic Exciton-Polariton Billiard. *Nature* (2015) 526:554–8. doi:10.1038/nature15522
170. Chen W, Kaya Özdemir Ş, Zhao G, Wiersig J, Yang L. Exceptional Points Enhance Sensing in an Optical Microcavity. *Nature* (2017) 548:192–6. doi:10.1038/nature23281
171. Romano S, Lamberti A, Masullo M, Penzo E, Cabrini S, Rendina I, et al. Optical Biosensors Based on Photonic Crystals Supporting Bound States in the Continuum. *Materials* (2018) 11:526. doi:10.3390/ma11040526
172. Romano S, Mangini M, Penzo E, Cabrini S, De Luca AC, Rendina I, et al. Ultrasensitive Surface Refractive index Imaging Based on Quasi-Bound States in the Continuum. *ACS Nano* (2020) 14:15417–27. doi:10.1021/acsnano.0c06050
173. Solomon ML, Saleh AAE, Poulikakos LV, Abendroth JM, Tadesse LF, Dionne JA. Nanophotonic Platforms for Chiral Sensing and Separation. *Acc Chem Res* (2020) 53:588–98. doi:10.1021/acs.accounts.9b00460
174. Koshelev K, Jahani Y, Tittl A, Altug H, Kivshar Y. Enhanced Circular Dichroism and Chiral Sensing with Bound States in the Continuum. In: *CLEO: QELS_Fundamental Science*. San Jose: Optical Society of America (2019). p. 6. FTh4C. doi:10.1364/CLEO\\text{_}QELS.2019.FTh4C.610.1364/cleo_qels.2019.fth4c.6
175. Zhang Z, Lan Z, Xie Y, Chen MLN, Sha WEI, Xu Y. Bound Topological Edge State in the Continuum for All-Dielectric Photonic Crystals. *Phys Rev Appl* (2021) 16:064036. doi:10.1103/physrevapplied.16.064036
176. Zhang Z, Qin F, Xu Y, Fu S, Wang Y, Qin Y. Negative Refraction Mediated by Bound States in the Continuum. *Photon Res* (2021) 9:1592. doi:10.1364/prj.427094
177. Lin Y, Feng T, Lan S, Liu J, Xu Y. On-chip Diffraction-free Beam Guiding beyond the Light Cone. *Phys Rev Appl* (2020) 13:064032. doi:10.1103/physrevapplied.13.064032
178. Yu Z, Xi X, Ma J, Tsang HK, Zou C-L, Sun X. Photonic Integrated Circuits with Bound States in the Continuum. *Optica* (2019) 6:1342. doi:10.1364/OPTICA.6.001342
179. Gong Z, Serafini J, Yang F, Preble S, Yao J. Bound States in the Continuum on a Silicon Chip with Dynamic Tuning. *Phys Rev Appl* (2021) 16:024059. doi:10.1103/PhysRevApplied.16.024059
180. Yu Y, Sakanas A, Zali AR, Semenova E, Yvind K, Mørk J. Ultra-coherent Fano Laser Based on a Bound State in the Continuum. *Nat Photon* (2021) 15:758–64. doi:10.1038/s41566-021-00860-5
181. Yu Z, Tong Y, Tsang HK, Sun X. High-dimensional Communication on Etchless Lithium Niobate Platform with Photonic Bound States in the Continuum. *Nat Commun* (2020) 11:2602. doi:10.1038/s41467-020-15358-x

Conflict of Interest: The authors declare that the research was conducted in the absence of any commercial or financial relationships that could be construed as a potential conflict of interest.